Received: 18 September 2020 | Revised: 12 November 2020 | Accepted: 21 November 2020

DOI: 10.1002/ardp.202000349

FULL PAPER

ARCH PHARM DPhG
Archiv der Pharmazie

Design, synthesis, in silico, and in vitro evaluation of 3-phenylpyrazole acetamide derivatives as antimycobacterial agents

Nikhil B. Gaikwad[1] | Krishna Nirmale[1] | Santosh K. Sahoo[1] | Mohammad N. Ahmad[2,3] | Grace Kaul[2] | Manjulika Shukla[2] | Srinivas Nanduri[1] | Arunava Das Gupta[2] | Sidharth Chopra[2] | Madhavi V. Yaddanapudi[1]

[1]Department of Pharmaceutical Technology and Process Chemistry, National Institute of Pharmaceutical Education and Research (NIPER), Hyderabad, Telangana, India

[2]Division of Microbiology, CSIR-Central Drug Research Institute, Lucknow, Uttar Pradesh, India

[3]Academy of Scientific and Innovative Research (AcSIR), Ghaziabad, Uttar Pradesh, India

Correspondence
Madhavi V. Yaddanapudi, Department of Pharmaceutical Technology and Process Chemistry, National Institute of Pharmaceutical Education and Research (NIPER), Balanagar, Hyderabad, Telangana 500037, India.
Email: yssmadhavi@gmail.com

Abstract

Mycobacterium tuberculosis (Mtb) is one of the most dangerous pathogens affecting immunocompetent and immunocompromised patients worldwide. Novel molecules, which are efficient and can reduce the duration of therapy against drug-resistant strains, are an urgent unmet need of the hour. In our current study, a series of new 2-(3-phenyl-1*H*-pyrazol-1-yl)acetamide and *N*′-benzylidene-2-(3-phenyl-1*H*-pyrazol-1-yl)acetohydrazide derivatives were designed, synthesized, and evaluated for their antimycobacterial potential. The biological evaluation revealed that **6b**, **6m**, **6l**, **7a**, and **7k** exhibited selective and potent inhibitory activity against Mtb. Furthermore, compounds **6m** and **7h** were found to be nontoxic to Vero cells with CC_{50} of greater than 20 and 80 mg/ml, respectively, and exhibited promising selectivity indices (SI) of greater than 666 and 320, respectively. All derivatives exhibited excellent ADME (absorption, distribution, metabolism, and excretion) properties in silico. Also, all the derivatives were found compliant with Lipinski's rule of five, showing their druggability profile. Molecular docking insights of these derivatives have shown outstanding binding energies on the mycobacterial membrane protein large transporters. These results indicate that this scaffold may lead to a potential antimycobacterial drug candidate in the discovery of antitubercular agents.

KEYWORDS

2-(3-phenyl-1*H*-pyrazol-1-yl)acetamide, acetamide, ADMET studies, antitubercular, *Mycobacterium tuberculosis*, pyrazole

1 | INTRODUCTION

Tuberculosis (TB), caused due to *Mycobacterium tuberculosis* (Mtb), is primarily a lung disease but can attack any part of the body such as the spine, brain, and kidney, hence causing extra-pulmonary tuberculosis.[1] In the majority of the patients, Mtb is present in a latent form (LTBI), which, in turn, transmutes into an active disease as soon as the patient's immunity gets weaker. However, people with LTBI remain a large human pool for TB, which implies that for the decline in the global TB burden, all forms of TB should be eradicated.[2] This is exemplified by the fact that big eight countries tally 67% of the total patients: India (27%), China (9%), Indonesia (8%), Pakistan (6%), Philippines (6%), Bangladesh (4%), Nigeria (4%), and South Africa (3%). WHO announced "The End TB strategy" to

eradicate TB from the world by 2035.[3] India's ambitious goal of ending TB by 2025 is larger and bigger, with India accounting for the majority of TB patients.[4] Among many factors, drug resistance is a big impediment in achieving the global targets in due time; thus there is an urgent unmet demand for newer, better, and novel antimycobacterials to overcome resistance and help eradicate TB.

Over the years, many scaffolds have been explored and developed against Mtb, that is, pyridine (isoniazid, ethionamide, and prothionamide), pyrazine (pyrazinamide and clofazimine), quinoline[5] (ofloxacin, levofloxacin, moxifloxacin and bedaquiline), isoxazolinone (linezolid, sutezolid, teriziidone, cycloserine, tedizolid, and LCB01–0371 [delpazolid]).[6,7] Many of these are given as first-line and second-line drugs for the treatment of TB but increasingly are facing resistance, due to which there is a negative impact on mortality and morbidity. Thus, the identification of new scaffolds is an urgent unmet requirement to combat drug resistance. One such scaffold is pyrazole, which in recent years has gained attention with its antitubercular potential.[8–13] Various antimycobacterial agents based on C3 and C5 substituted phenylpyrazole derivatives have been reported previously.[10,12–14] Compound **I** (Figure 1) with InhA inhibition activity was found active against both sensitive as well as drug-resistant Mtb strains.[15] 3-(4-Chlorophenyl) pyrazole derivative **II** (Figure 1) carrying a substituted azetidinone moiety demonstrated submicromolar activity.[14] Quinolinyl pyrazole hybrids, such as **III**, illustrated excellent antitubercular activity[16,17] and quinoline-based hybrid derivatives with pyrazole have also shown promising antitubercular activity.[18] Hybrid molecules based on pyrazole and triazole moiety linked with acetamide (**IV**) (Figure 1) were reported to inhibit nonpathogenic *Mycobacterium smegmatis*.[9] Quinazoline- and benzimidazole-based acetamide derivative **V** (Figure 1) was reported earlier with antimycobacterial activity.[19] Also, another interesting amide-based pyrazole derivative called rimonabant (Figure 1), a CB1 receptor modulator was found to have antimycobacterial activity, acting as an MmpL3 inhibitor. Further, the derivatives of rimonabant were found to have a better potency than rimonabant.[20] Antitubercular agents based on cyclohexyl-indole-2-carboxamide were reported in 2013.[21] These derivatives were proved to be the primary hits, which led to more potent derivatives reported later.[22,23] With regard to the biological significance of an acetamide bridge between pyrazole and amine in antimycobacterial activity and also as a part of our ongoing research on pyrazole-based antimycobacterial agents, we have proposed a new composite structure of 2-(3-phenyl-1*H*-pyrazol-1-yl)acetamide followed by its antimycobacterial evaluation. The rationale behind the design was based on the exceptional activity reported for the repurposed drug rimonabant on the MmpL3 receptor. But molecules with a low selectivity index (SI) may be harmful to the central nervous system (CNS). The diaryl moieties of rimonabant made the molecule hydrophobic because of which it passes the blood–brain barrier (BBB). Hence, we have modified the scaffold with a single aromatic ring, and acetohydrazone was chosen as the linker bridge, which rightfully fits between an amine and pyrazole moiety with moderate hydrophilicity along with good binding interactions of the molecule. Hence, substituted phenyl pyrazolyl acetohydrazones were designed and synthesized (Figure 2). But the synthesized molecules were found inactive against the ESKAP panel and Mtb H37Rv. Hence, the scaffold was further modified and the acetohydrazone linker was replaced with acetamide (Figure 2). The synthesized pyrazole-based acetamides were tested against the ESKAP pathogen panel and Mtb H37Rv. Many of the compounds showed excellent activity, which helped

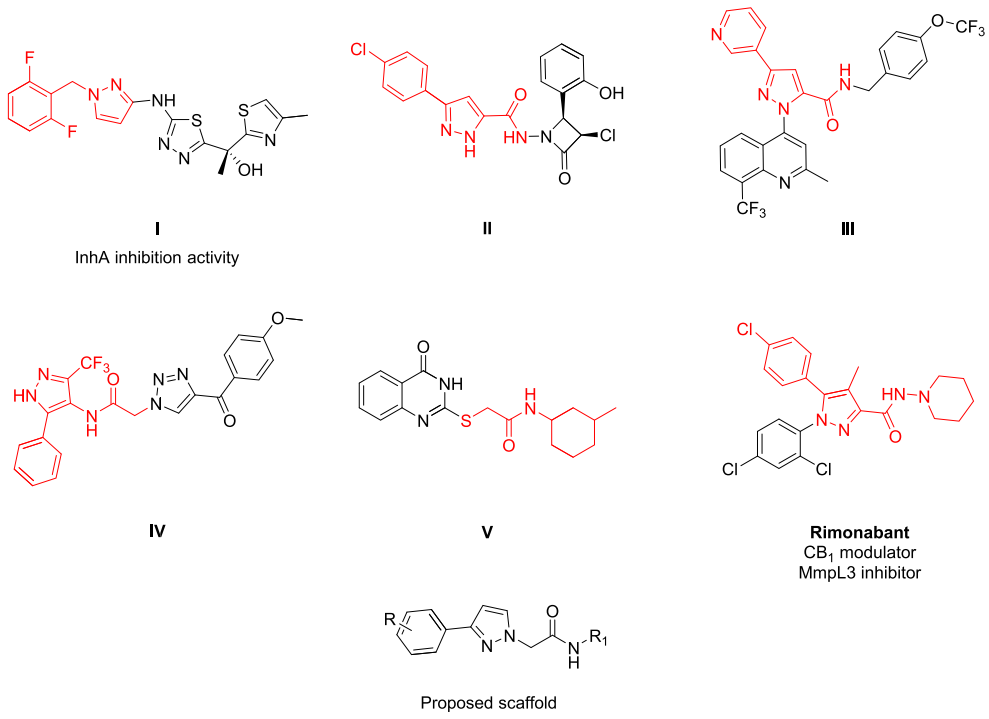

FIGURE 1 Pyrazole and acetamide scaffolds with antimycobacterial activity along with the proposed hybrid pyrazole acetamide scaffold

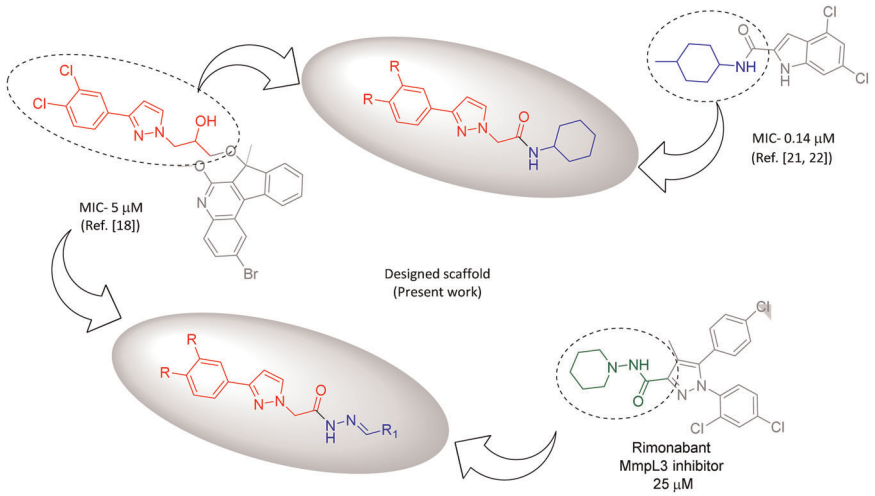

FIGURE 2 The rationale for the design of 2-(3-phenyl-1*H*-pyrazol-1-yl)acetamide derivatives as a new antitubercular agent

to evaluate the primary structural prerequisite for the potency of compounds (structure–activity relationship [SAR]). The most active molecules were additionally tested against a panel of drug-resistant strains of Mtb H37Rv and cytotoxicity against Vero cells to determine their drug-like potential. Further literature scouting on the proposed structure illustrated that there are no reports available on 2-(3-phenyl-1*H*-pyrazol-1-yl)acetamide framework with anti-Mtb properties.

2 | RESULTS AND DISCUSSION

2.1 | Chemistry

Designed molecules were synthesized, as shown in Scheme 1. All schemes have common starting material, which is substituted ethyl 2-(3-phenyl-1*H*-pyrazol-1-yl)acetate. The series **6** and **7** were synthesized in two important steps, mainly generation of 2-(3-phenyl-1*H*-pyrazol-1-yl)acetic acid and finally acid-amine coupling to get acetamide derivatives (Scheme 1), although generation of the acid group involves four substeps. In the first step, respective nitroacetophenones were converted to dimethylamino enaminones (**1**) by using *N*,*N*-dimethylformamide dimethyl acetal by the reported procedure.[24] Pyrazole derivatives (**2**) were obtained from substituted enaminones when treated with 35% hydrazine hydrate in the presence of ethyl alcohol in good yields.[25] The obtained pyrazole **2** was alkylated with ethyl bromoacetate in the presence of potassium carbonate in *N*,*N*-dimethylformamide, and stirring for 72 h at 70°C as per the reported protocols, which gave a white solid product with 90–92% yields.[26,27] The acetate obtained was hydrolyzed by using lithium hydroxide in tetrahydrofuran and water mixture in a 1:1 ratio at room temperature for 20 h to yield the desired 2-(3-nitrophenyl-1*H*-pyrazol-1-yl)acetic acid with 98% yield.[27] Lastly, 2-(3-phenyl-1*H*-pyrazol-1-yl)acetic acid was coupled with different amine groups to yield acetamide derivatives as a final product. 1-Ethyl-3-(3-dimethylaminopropyl)carbodiimide (EDC.HCl) along with 4-dimethylaminopyridine (DMAP) was used as a coupling

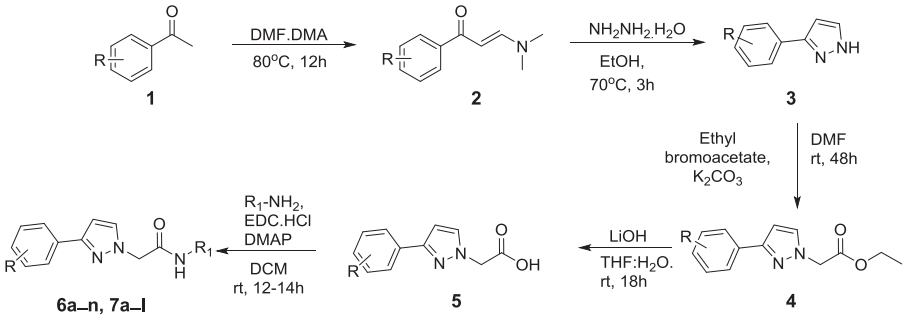

6a: R- 4-NO_2, R_1- 4-(Trifluoromethyl)aniline
6b: R- 4-NO_2, R_1- Cyclohexyl
6c: R- 4-NO_2, R_1- Cycloheptyl
6d: R- 4-NO_2, R_1- 3-Chloroaniline
6e: R- 4-NO_2, R_1- 3-Chloro-4-fluoroaniline
6f: R-4-NO_2, R_1- Anisidine
6g: R- 4-NO_2, R_1- 2-Fluoroaniline
6h: R-4-NO_2, R_1- 4-Fluoroaniline
6i: R- 4-NO_2, R_1- 1-Naphthylamine
6j: R- 4-NO_2, R_1- 4-Bromoaniline
6k: R- 4-NO_2, R_1- Aniline
6l: R- 4-NO_2, R_1- 4-Morpholinoaniline
6m: R- 4-NO_2, R_1- 4-Chloroaniline
6n: R- 4-NO_2, R_1- 2,4,6-Trimethylaniline

7a: R- 3-NO_2, R_1- Cyclopropyl
7b: R- 3-NO_2, R_1- Cyclohexyl
7c: R- 3-NO_2, R_1- Cycloheptyl
7d: R- 3-NO_2, R_1- 3-Chloroaniline
7e: R- 3-NO_2, R_1- 3-Chloro-4-fluoroaniline
7f : R- 3-NO_2, R_1- Anisidine
7g: R- 3-NO_2, R_1- 2-fluoroaniline
7h: R- 3-NO_2, R_1- 4-fluoroaniline
7i : R- 3-NO_2, R_1- 1-Naphthylamine
7j : R- 3-NO_2, R_1- 4-Bromoaniline
7k: R- 3-NO_2, R_1- 3-Nitro-4-fluoroaniline
7l : R- 3-NO_2, R_1- Benzothiazole

SCHEME 1 Synthetic route to compounds of series **6** and **7**

agent, leading to products with 61–87% yields (Figure 3). In series **9**, **10**, and **11**, ester **4** was converted to respective pyrazolyl acetohydrazides (Scheme 2). The final step involves the conversion of acetohydrazides to hydrazones by the reaction of substituted aldehydes (Figure 4) in the presence of catalytic acetic acid in ethanol. It is significant to refer that amine substituents and aldehyde for each series were selected based on excellent antimycobacterial results reported in the literature.[28,29] Spectroscopic and spectrometric data were acquired for all the synthesized compounds (presented in Supporting Information).

To exemplify, one of the potent derivatives **6m** in ^{1}H NMR (nuclear magnetic resonance) has shown distinctive sharp singlet peaks of the methylene proton and amide proton at 5.15 and 10.57 ppm, respectively, which ensured the formation of amide –NH– bond. The proton of pyrazole C-5 –CH- appeared as a doublet at 7.93 ppm and also pyrazole C-4 –CH– proton appeared as a doublet at 6.99 ppm. Protons on phenyl ring attached to pyrazole appeared as a doublet at 8.26 and 8.08 ppm belonging to *meta* and *ortho* to pyrazole substitution, respectively; similarly, phenyl ring protons *ortho* and *meta* to amine also appeared as doublets at 7.65 and 7.41 ppm, respectively. Likewise, ^{13}C NMR interpretation of derivative **6m** designates the existence of carbonyl carbon of the amide group at 165.8 ppm. The methylene (–CH_2–) carbon bridging amide and pyrazole was observed at 79.6 ppm. C-3, C-4, and C-5 pyrazole carbon appeared correspondingly at 148.9, 104.8, and 127.7 ppm. Remaining carbons at the *ipso*, *ortho*, *meta*, and *para* positions of the phenyl ring attached to pyrazole appeared at 146.8, 126.3, 124.6, and 140.1 ppm, respectively. Lastly, the *ipso*, *ortho*, *meta*, and *para* carbons of the phenyl ring attached to amine were observed at 137.9, 121.2, 129.3, and 134.7 ppm, respectively.

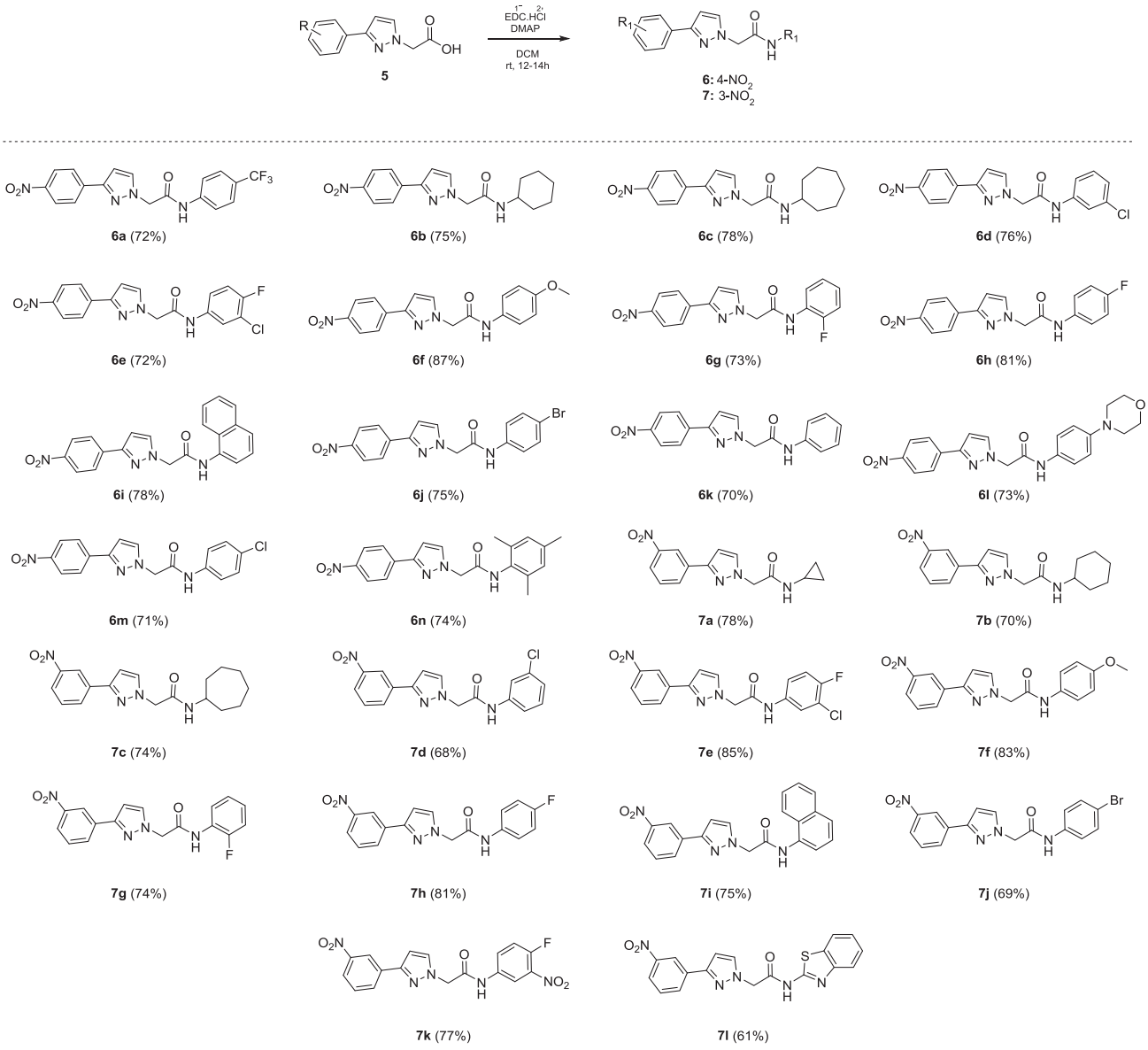

FIGURE 3 Synthesized molecules of series **6** and **7** with their respective yields

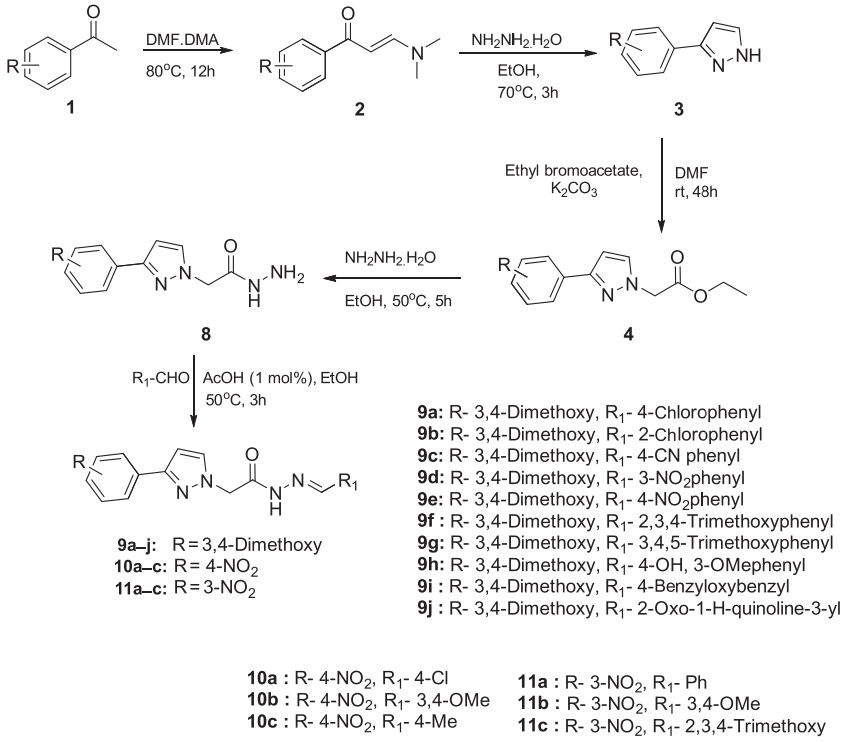

SCHEME 2 Synthetic route to compounds of series **9**, **10**, and **11**

^{1}H NMR for the compound **9c** from the hydrazone series showed two singlets of the characteristic methyl of the dimethoxy group at 3.78 and 3.81 ppm. The singlet of the –NH– of the hydrazide group was present at 11.93 ppm along with –CH– of the amine group at 8.09 ppm, which confirmed the synthesis of the hydrazone moiety. The two hydrogens from –CH_2– of the acetamide were observed at 5.46 ppm as a singlet. The rest of the aromatic protons of pyrazole appeared as doublets at 6.70 and 7.77 ppm, which correspond to hydrogens at fourth and fifth position of pyrazole, respectively, and the aromatic protons were present as doublets at 6.97 and 7.31 ppm, depicting fifth and sixth position, respectively, and a singlet at 7.33 ppm depicting second position of the phenyl ring attached to pyrazole. Two doublets at 7.91 and 7.95 ppm correspond to *meta* and *ortho* protons of the hydrazine phenyl ring. Finally, all the acetamide derivatives were characterized by ^{1}H, ^{13}C NMR, high-resolution mass spectrometry (HRMS), and Fourier transform infrared spectrometry (FTIR) and are in accordance with the pertinent structures as presented in the experimental section. The HRMS (electrospray ionization) data of each compound represented as an $[M+H]^+$ or $[M+Na]^+$ peaks comply with their precise molecular formula.

2.2 | Pharmacology/biology

2.2.1 | *M. tuberculosis* H37Rv inhibition studies

All synthesized derivatives **6a–n**, **7a–l**, **9a–j**, **10a–c**, and **11a–c** were assessed for their antibacterial activity against ESKAP pathogen panel by using broth microdilution assay as well as against Mtb H37Rv and other mycobacterial pathogens (nontuberculous mycobacteria [NTM]) by using a whole-cell assay with isoniazid (INH), rifampicin (RIF), and levofloxacin (LEVO) as reference. All the molecules of the five series were found inactive on the ESKAP pathogen panel, except compound **11c**, which showed a minimum inhibitory concentration (MIC) of 32 μg/ml on *Staphylococcus aureus;* due to less potency, this molecule was not considered for further studies. Further antimycobacterial screening displayed that all molecules of the series **6** and **7** demonstrated good to excellent activity against Mtb and moderate activity against NTM and were ineffective against ESKAP pathogen panel, suggesting the selective inhibition of designed molecules toward slow-growing mycobacteria (Table 1). Upon analysis, cycloalkyl amide derivatives were found to have excellent activity than corresponding aromatic amide derivatives. The antimycobacterial activity was found to be dependent on the substituents on the amine group and position of nitro group on phenyl ring attached to the pyrazole acetic acid. Cyclopropyl, cyclohexyl, and cycloheptyl amides were studied and all three were found to have excellent activity against Mtb but their activities against NTM pathogens varied with ring size. Cyclohexyl and cyclopropyl amide derivatives of respective series exhibited activity against Mtb, *M. fortuitum*, and *M. chelonae* with MIC comparable to the reference compound (isoniazid, levofloxacin, and rifampicin) used for testing (Table 2). Although cycloheptyl amide derivatives **6c** and **7c** of both series were active on Mtb but found inactive against NTM pathogens. This suggested that the ring size was affecting the selectivity against these strains. Moreover, in aromatic amide derivatives, substituents on the phenyl ring were crucial for activity. Variations in aromatic acetamide derivatives were studied by using electron-withdrawing, electron-donating, or aliphatic group substitutions at different positions of a phenyl group attached to amine, which led to molecules with good to excellent anti-TB activity and the positions of these substituents on the phenyl ring were found to be crucial for activity. *Para*-substituted derivatives **6a**, **6e**, **6f**, **6h**, **6k**, **6m**, **7f**, and **7h**

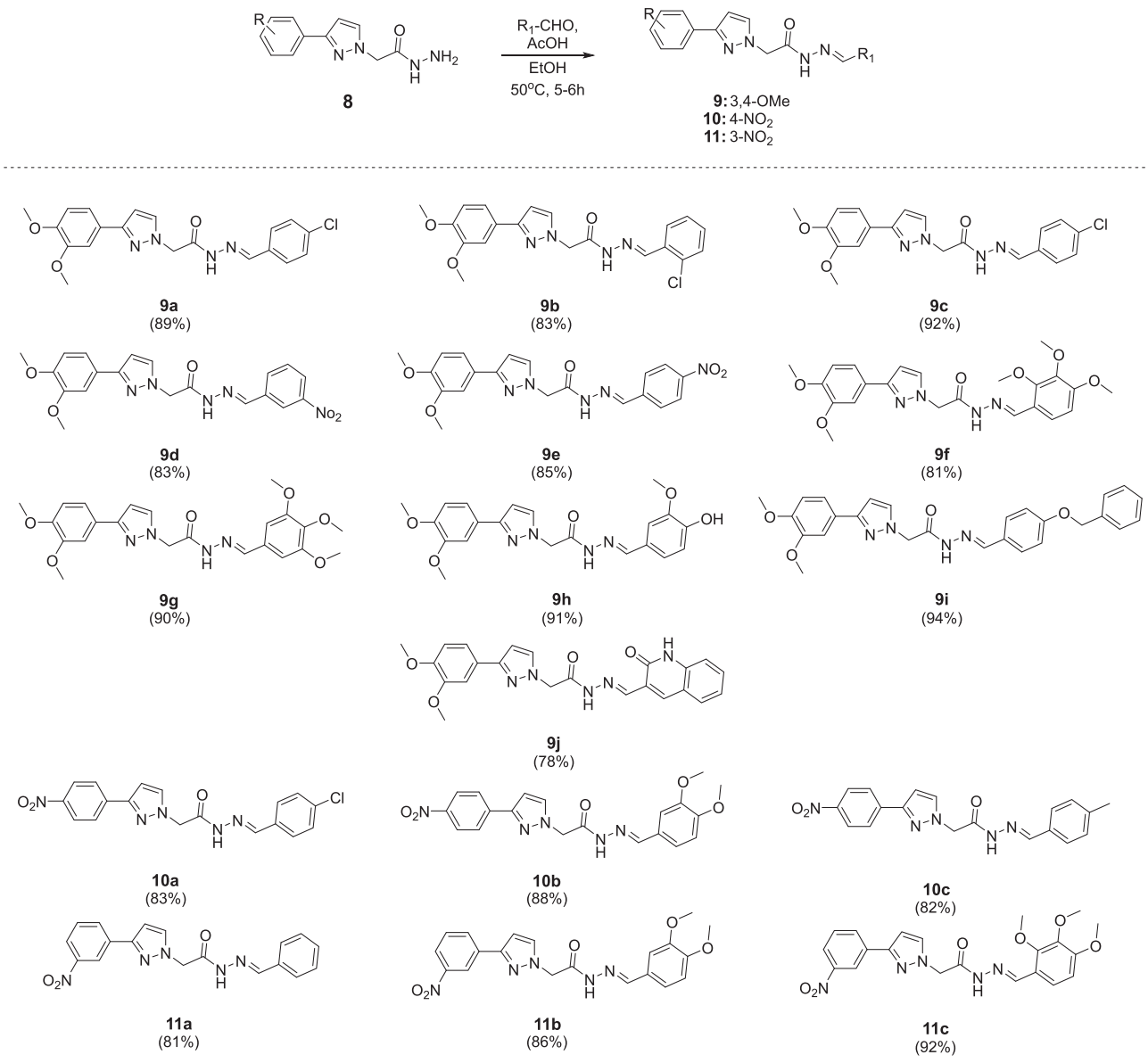

FIGURE 4 Synthesized molecules of series **9**, **10**, and **11** with their respective yields

were well tolerated for activity compared to *ortho*- and *meta*-substituted derivatives. It is noteworthy that any substitution on *meta* position reduced antimycobacterial potential and *ortho* substitution leads to complete loss of activity. In summary, aromatic derivatives displayed lesser potency as compared to aliphatic derivatives, disubstituted derivatives exhibited similar results to those of monosubstituted derivatives. Despite having identical substitutions, **6e** and **7e** displayed disparate activity, showing that the position of nitro group on pyrazole ring had significant influence in determining activity. *Meta* nitro derivative **7e** had excellent activity against Mtb H37Rv compared to **6e** but was inactive against NTM strains. Unlike **6e**, when the chloro group of **7e** was replaced by the NO_2 group in **7k**, it was found to elevate potency. To study the significance of hydrophobic moieties, naphthylamine, aniline, and trifluoromethylaniline acetamides were evaluated (compounds **6i**, **6l**, **6o**, and **7i**), which displayed MIC > 64 μg/ml, which indicates that cycloalkyl amines are more effective than alkyl and aromatic amines. The correlation of ClogP and MIC values are given in Figure 5. The position of the nitro group also affects the activity, which was studied by shifting the position of the nitro group from *para* to *meta* in **6c** and **6f** compounds, which, in turn, led to partial to complete loss of activity, indicating the importance of the group and its position. The SAR parameters discussed are summarized below (in Figure 6).

2.2.2 | Cytotoxicity against Vero cells

A cytotoxicity assay was performed against Vero cells (African green monkey kidney cell line; ATCC CCL-81) using MTT assay (3-(4,5-dimethylthiazol-2-yl)-2,5-diphenyltetrazolium bromide) to assess the

TABLE 1 Minimum inhibitory concentration (mg/ml) of 2-[3-(4-nitrophenyl)-1*H*-pyrazol-1-yl]acetamides **6a–n** and 2-[3-(3-nitrophenyl)-1*H*-pyrazol-1-yl]acetamides **7a–l** against ESKAP pathogen panel and *Mycobacterium tuberculosis*

	Gram +ve	Gram −ve				
	Staphylococcus aureus	*Escherichia coli*	*Klebsiella pneumoniae*	*Acinetobacter baumannii*	*Pseudomonas aeruginosa*	*Mycobacterium tuberculosis*
Entry	ATCC 29213	ATCC 25922	BAA 1705	BAA 1605	ATCC 27853	H37Rv
6a	>64	>64	>64	>64	>64	0.06
6b	>64	>64	>64	>64	>64	0.06
6c	>64	>64	>64	>64	>64	0.06
6d	>64	>64	>64	>64	>64	>64
6e	>64	>64	>64	>64	>64	16
6f	>64	>64	>64	>64	>64	0.12
6g	>64	>64	>64	>64	>64	>64
6h	>64	>64	>64	>64	>64	0.12
6i	>64	>64	>64	>64	>64	4
6j	>64	>64	>64	>64	>64	>64
6k	>64	>64	>64	>64	>64	>64
6l	>64	>64	>64	>64	>64	0.06
6m	>64	>64	>64	>64	>64	0.06
6n	>64	>64	>64	>64	>64	>64
7a	>64	>64	>64	>64	>64	0.12
7b	>64	>64	>64	>64	>64	0.06
7c	>64	>64	>64	>64	>64	>64
7d	>64	>64	>64	>64	>64	>64
7e	>64	>64	>64	>64	>64	0.06
7f	>64	>64	>64	>64	>64	>64
7g	>64	>64	>64	>64	>64	>64
7h	>64	>64	>64	>64	>64	0.25
7i	>64	>64	>64	>64	>64	>64
7j	>64	>64	>64	>64	>64	>64
7k	>64	>64	>64	>64	>64	0.12
7l	>64	>64	>64	>64	>64	>64
9a	>64	>64	>64	>64	>64	>64
9b	>64	>64	>64	>64	>64	>64
9c	>64	>64	>64	>64	>64	>64
9d	>64	>64	>64	>64	>64	>64
9e	>64	>64	>64	>64	>64	>64
9f	>64	>64	>64	>64	>64	>64
9g	>64	>64	>64	>64	>64	>64
9h	>64	>64	>64	>64	>64	>64
9i	>64	>64	>64	>64	>64	>64
9j	>64	>64	>64	>64	>64	>64
10a	>64	>64	>64	>64	>64	>64

(Continues)

TABLE 1 (Continued)

Entry	Gram +ve *Staphylococcus aureus* ATCC 29213	Gram −ve *Escherichia coli* ATCC 25922	*Klebsiella pneumoniae* BAA 1705	*Acinetobacter baumannii* BAA 1605	*Pseudomonas aeruginosa* ATCC 27853	*Mycobacterium tuberculosis* H37Rv
10b	>64	>64	>64	>64	>64	>64
10c	>64	>64	>64	>64	>64	>64
11a	>64	>64	>64	>64	>64	>64
11b	>64	>64	>64	>64	>64	>64
11c	**32**	>64	>64	>64	>64	>64
Levofloxacin	<0.5	<0.5	64	8	1	NT
Isoniazid	NT	NT	NT	NT	NT	0.06
Rifampicin	NT	NT	NT	NT	NT	0.03

Abbreviation: NT, not tested.

effect of active derivatives **6b**, **6f**, **6h**, **6l**, **6m**, **7a**, **7b**, **7h**, and **7k** on mammalian cells. The results were denoted as CC_{50}, that is, the lowest concentration of test compound which results in a 50% reduction in cell viability. All the test samples were tested in triplicate and doxorubicin was used as a reference. Cytotoxicity examination revealed that **6b**, **6f**, **6h**, **6l**, **6m**, **7a**, **7h**, and **7k** were found to be nontoxic to Vero cells (CC_{50} were ≥05 to ≥10 mg/ml) and exhibited a promising SI of ≥10 to ≥666. These observed results are presented in Table 3.

2.3 | In silico studies

2.3.1 | Molecular docking studies

Exemplary mycobacterial inhibition inspired us to investigate the binding pattern of these molecules by using molecular docking studies to understand the molecular requirements for the biological activity. Thus, the structural features and previous reports on pyrazoles[30–33] and especially amide derivatives[34,35] like rimonabant formed the basis for the design of these molecules. Rimonabant is a repurposed drug for tuberculosis, which is a pyrazole derivative with amide functionality inhibiting the MmpL3 receptor. All designed derivatives that were found active on Mtb H37Rv were screened on all the transmembrane receptors of the *M. tuberculosis* (KasA, DprE1, InhA, and MmpL3). These proteins play a crucial role in the biosynthesis as well as transportation of mycolic acid in Mtb. Docking studies were performed on four PDB IDs of each receptor protein, KasA (PDB ID: 5W2Q), DprE1 (PDB ID: 4P8H), InhA (PDB ID: 4TZK), and MmpL3 (PDB ID: 6ajj) (docking results included in the Supporting Information). The molecular docking results on all these receptor proteins revealed that the acetamide derivatives have a lesser binding affinity toward KasA and DprE1 proteins and moderate binding affinity toward InhA protein and best affinity toward MmpL3 receptor. After the results of molecular docking on InhA and MmpL3 proteins, the antimycobacterial potencies of respective molecules were assessed. The MmpL3 docking scores were found to be in line with the biological activity. The molecular insights of acetamide derivatives revealed that the pyrazole ring has hydrophobic π–π stacking interaction with TYR646 of MmpL3 protein. The amide –NH– group has a hydrogen bond with the ASH645; along with it, the phenyl ring on amine has π–π stacking and π–cation interactions with PHE649 and PHE260. The nitrophenyl ring on the pyrazole is found to enhance the binding of the molecules to the receptor pocket by forming a hydrogen bond with ARG653 and THR289 amino acids of backbone protein. The phenyl ring attached to the pyrazole ring was found to form the π–π stacking interactions with TYR257, and the nitro group had hydrogen bonding with THR289 through oxygen and π–cation interaction with PHE260 through nitrogen. Also, the majority of molecules have charged negative interactions with ARG653 and charged positive interactions with ASH256 and ASH645 (few molecules with GLU647), also glycine interactions with GLY641, GLY252, GLY258. The compounds were found to establish hydrophobic (nonpolar) interactions with PHE260, TYR257, ILE253, LEU686, LEU708, ILE249, ALA637, VAL638, LEU642, TYR646, ILE297, VAL648, PHE649, VAL290, and hydrophilic polar interactions with SER293, SER300, SER301, THR289, THR644, SER643, SER263, and SER286 amino acid residues of the protein (Figure 7a–c). To comprehend the detailed outcomes, the most active ligand of each series **6a** and **7a** were superimposed and the resultant poses disclosed that the structural features of both series were superimposed similarly to each other, signifying the probable binding modes of these molecules. The nitro group position on both these series was different, which led to a different interaction of the nitro group of *meta* derivative, that is, series **7** molecules. Other interactions were found correlating to each other in both the series. The consequent superimposed poses of the potent ligand **6a** and **7a** suggested that acetamide functionality of **7h** engaged identically to **6m** acetamide group (Figure 7e). The docking scores, along with their bonding aspects, are presented in Table 4.

TABLE 2 In vitro activities of 2-[3-(4-nitrophenyl)-1*H*-pyrazol-1-yl]acetamides **6a–n** and 2-[3-(3-nitrophenyl)-1*H*-pyrazol-1-yl]acetamides **7a–l** against *Mycobacterium tuberculosis* H37Rv, *M. abscessus*, *M. fortuitum*, *M. chelonae*, and ClogP values correlation

Entry	ClogP[a]	Minimum inhibitory concentration			
		H37Rv	*M. abscessus*	*M. fortuitum*	*M. chelonae*
6a	4.43	0.06	>64	>64	>64
6b	3.27	0.06	>64	1	1
6c	3.83	0.06	>64	>64	>64
6d	4.07	>64	>64	>64	>64
6e	4.30	16	>64	16	32
6f	3.17	0.12	>64	2	4
6g	3.50	>64	>64	>64	>64
6h	3.50	0.12	>64	2	2
6i	4.27	>64	>64	>64	>64
6j	4.22	>64	>64	>64	>64
6k	3.09	>64	>64	>64	>64
6l	2.55	0.06	>64	1	1
6m	4.07	0.06	>64	1	2
6n	3.29	>64	>64	>64	>64
7a	1.83	0.12	>64	2	2
7b	3.27	0.06	>64	1	1
7c	3.83	>64	>64	>64	>64
7d	4.07	>64	>64	>64	>64
7e	4.30	0.06	>64	>64	>64
7f	3.17	>64	>64	2	2
7g	3.50	>64	>64	>64	>64
7h	3.50	0.25	>64	8	8
7i	4.27	>64	>64	>64	>64
7j	4.22	>64	>64	>64	>64
7k	3.33	0.12	>64	2	2
7l	3.93	>64	>64	>64	>64
Levofloxacin	−0.51	NT	1	0.03	0.03
Rifampicin	-	0.06	NT	NT	NT
Isoniazid	−0.67	0.03	NT	0.5	0.5

Abbreviation: NT, not tested.

[a]ClogP were calculated by ChemBioDraw Ultra, version 14.0.0.117.

2.3.2 | Prediction of ADME (absorption, distribution, metabolism, and excretion) properties

To establish the drug likeliness topographies, ADME parameters of designed pyrazole acetamides were determined by using the QikProp module of the Schrödinger suite. A large margin of drugs have the physicochemical properties in a certain range, such as hydrogen-bond acceptor (accept HB) 2–20, hydrogen-bond donor (donors HB) 0–6, molecular weight 130–725, and predicted QP logPo/w −2 to 6.5.[36] The projected drug likeness properties of all the derivatives were found to be within the mentioned standard parameters. Lipinski's rule is the most frequently used thumb rule to decide the drug likeness of the molecules. The rule illustrates molecular features that are significant for pharmacokinetics of desired molecules in the human body, based on their absorption, distribution, metabolism, and excretion (ADME). Most recently, T is inserted at the end and that becomes ADMET in which T denotes the toxicity profile of the drug molecule. According to Lipinski's rule, physicochemical descriptors should be within the range, like logP values should be less than or equal to 5, molecular weight less

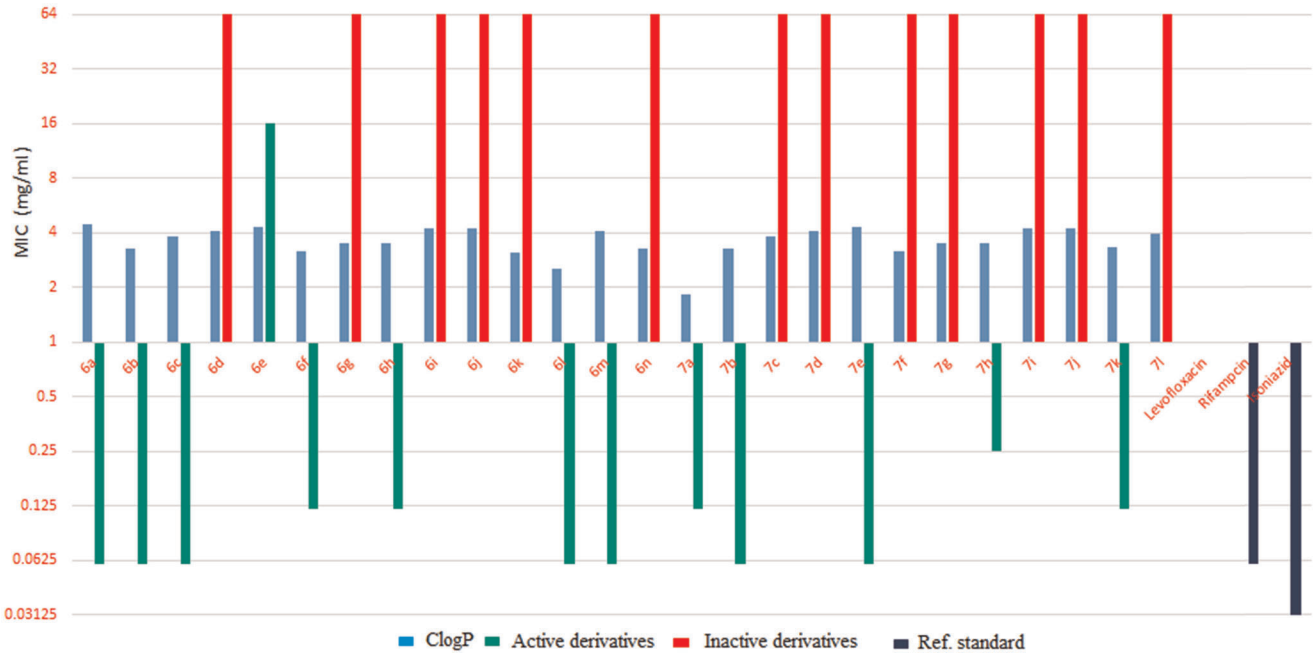

FIGURE 5 Correlation between minimum inhibitory concentration (MIC) and ClogP values of pyrazole series

than or equal to 500, H-bond acceptor ≤ 10, and H-bond donors ≤ 5. Thus, the molecule not obeying two or more of these parameters will lead to poor absorption or permeation.[37,38] When all the 26 compounds were studied for the Lipinski rule of five, it was observed that all 26 compounds did not violate any parameters. QPPCaco is a parameter to predict Caco-2 cell permeability of molecule in nm/s (>500 is great absorption, <25 is poor absorption). It is the human absorption process by the nonactive transport mechanism across the gut–blood barrier.[39] The predicted QPPCaco value for acetamide derivatives illustrates that designed compounds certainly absorb through the gut layer. For the target molecule to become CNS active, it must have the CNS value more than or equal to 2 (−2 [inactive] to +2 [active]).[39,40] The predicted value for the CNS was in the range of −1 to −2, thus indicating that these molecules would be inactive on CNS. The logBB values help to determine the distribution of the compound in the brain. If the compound is having a log BB greater than 0.3 it will cross the BBB, and if it is less than −1.0 those compounds will be weakly distributed to the brain. The Qikprop determined logBB value of the selected molecules was in the range of −1 to −2, which suggested that these compounds will not cross the BBB; thus, no central nervous system activity will be observed. Furthermore, the QPlog HERG value denotes the predicted IC_{50} value for the blockage of HERG K+ channels. Designed compounds demonstrated good

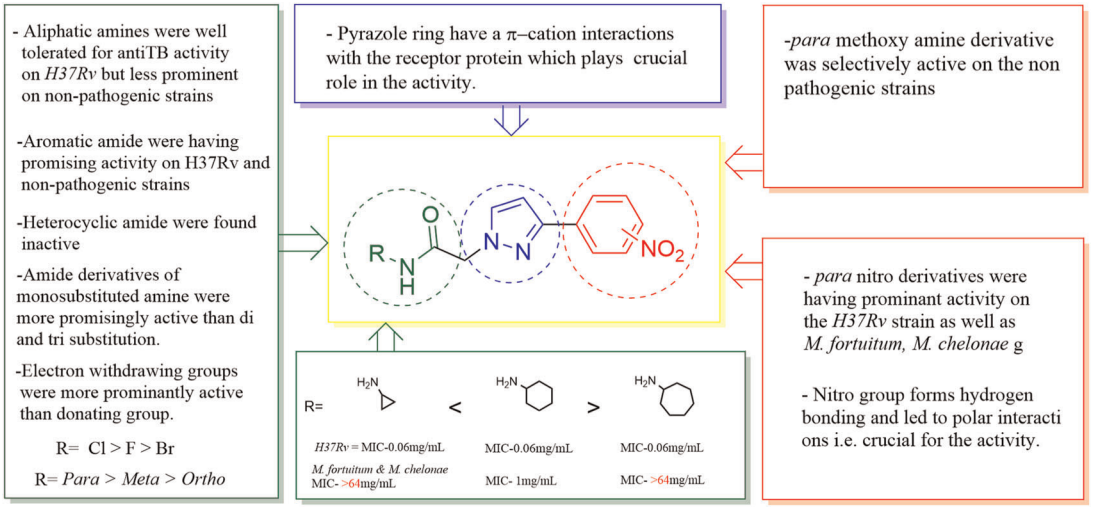

FIGURE 6 Structure–activity relationship of acetamide derivatives of pyrazole

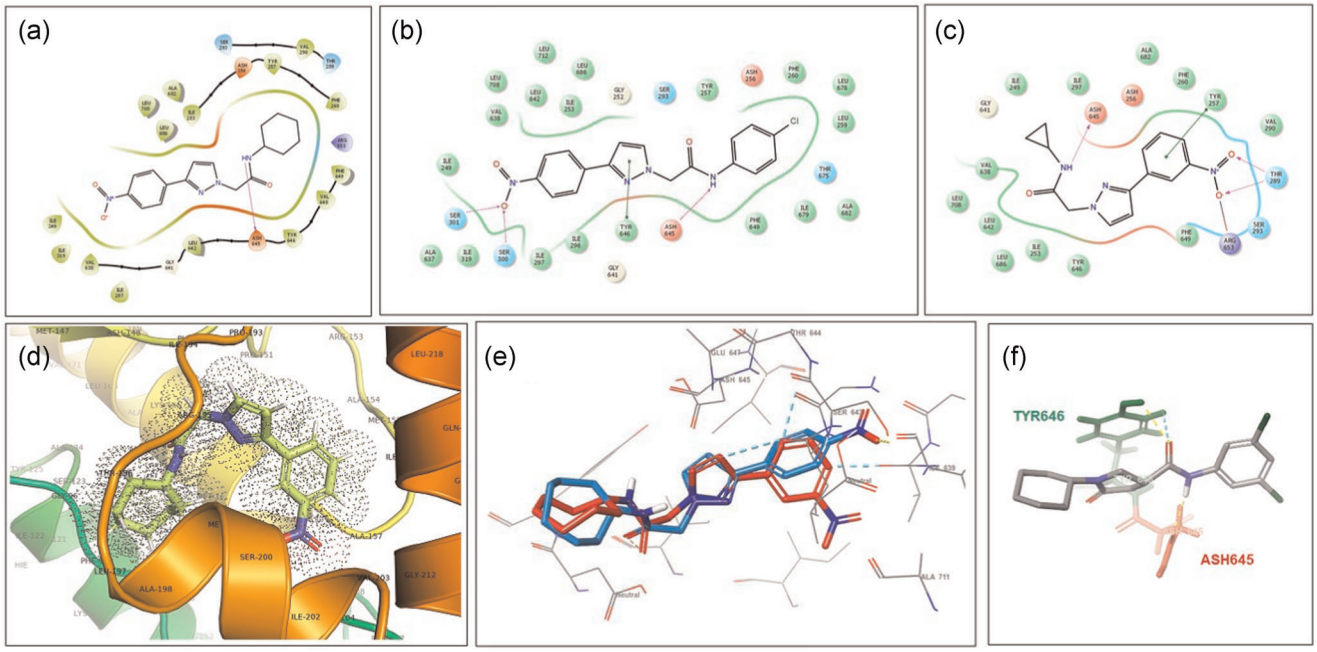

FIGURE 7 (a) Compound **6a** molecular binding interactions with the binding site pocket. The pink solid arrow represents the H-Bond interaction with the receptor protein backbone. (b) Compound **6m** interactions with the binding site pocket. The green solid line represents π–π stacking interactions. (c) Compound **7a** molecular binding interactions with the binding site pocket. The pink solid arrow represents the H-bond interaction with the receptor protein backbone. (d) Compound **7b** in the binding pocket of MmpL3 protein. (e) Molecular docking representation showing the superimposition of **6a** (blue) and **7a** (red) ligand interactions in receptor binding pocket of MmpL3 protein (PDB ID: 6ajj). Dashed lines represent hydrogen bonds. (f) Interactions of reference ligand in the binding pocket, the hydrogen bond between amide –NH– and ASH645 and C═O and TYR646

predicted pharmacological properties like HERG K+ channel (HERG K+), QPlogKhsa, which predicts binding to human serum albumin, QPPMDCK predicts MDCK cell permeability. MDCK cells are good mimic for the BBB, and QP logKp predicts the skin permeability of the molecule. Also, the percent absorption values of the majority of the compounds were found to be in the range of 85–100. Only one compound had a % absorption of 78% (**7a**), which is because of the aliphatic ring present in the molecule. Values of predicted descriptors are presented in Table S2 in ESI. The predicted values of the descriptors suggest that all the compounds were following good ADME properties. The active molecules of both series were showing a good ADME profile, which suggests that these molecules can be taken for further biological evaluation to develop potential antitubercular agents.

TABLE 3 Cytotoxicity profile against Vero cells and selectivity index (SI) of selected compounds on various mycobacterial strains

Entry	CC_{50} (μg/ml)	*Mycobacterium tuberculosis*		*Mycobacterium fortuitum*		*Mycobacterium chelonae*	
		MIC (μg/ml)	SI (CC_{50}/MIC)	MIC	SI	MIC	SI
6b	>10	0.06	>166	1	>10	1	>10
6f	20	0.125	160	2	10	4	5
6h	>20	0.125	>160	2	>10	2	>10
6l	>10	0.06	>166	1	>10	1	>10
6m	>20	0.06	>666	1	>20	2	>10
7a	>20	0.12	>166	2	>10	2	>10
7b	>6.25	0.06	>104	1	>6.25	1	>6.25
7h	>80	0.25	>320	8	>10	8	>10
7k	>20	0.12	>166	2	>10	2	>10

Abbreviation: MIC, minimum inhibitory concentration.

TABLE 4 Docking scores, binding energy, H-bond interactions for few potent acetamide derivatives

Entry	Docking score	Binding energy	H-Bonding	
			Ligand	Amino acid
6l	−10.569	−60.422	Amide –N–H	ASH645
6h	−10.372	−73.17	Amide –N–H	ASH645
6i	−11.915	−83.349	Amide –N–H	ASH645
6l	−10.569	−60.422	Amide –N–H	ASH645
6m	−10.972	−73.161	Amide –N–H	ASH645
7a	−8.497	−56.445	Amide –N–H	ASH645
			Nitro –N═O	THR289, ARG653
7h	−10.445	−81.294	Amide –N–H	ASH645
			Nitro –N═O	THR289, GLY192
7i	−11.915	−83.349	Amide –N–H	ASH645
7l	−10.538	−78.289	Amide –N–H	ASH645
			Nitro –N═O	ARG653, THR289
Cocrystal ligand	−11.980	−43.067	Amide –N–H	ASH645

3 | CONCLUSION

In summary, a new series of compounds based on 2-[3-(4-nitrophenyl)-1*H*-pyrazol-1-yl]acetamides **6a–n**, 2-[3-(3-nitrophenyl)-1*H*-pyrazol-1-yl] acetamides **7a–l**, *N*′-benzylidene-2-[3-(3,4-dimethoxyphenyl)-1*H*-pyrazol-1-yl]acetohydrazides **9a–j**, *N*′-benzylidene-2-[3-(4-nitrophenyl)-1*H*-pyrazol-1-yl]acetohydrazides **10a–c**, *N*′-benzylidene-2-[3-(3-nitrophenyl)-1*H*-pyrazol-1-yl]acetohydrazides **11a–c** were designed, synthesized, and their in vitro antimycobacterial activity and the cytotoxicity in Vero cells was evaluated. The synthesis of these molecules is simple and effortless with readily available reactants, a painless method of purification, and a satisfying amount of yields, which makes the scheme attractive. Furthermore, many of the synthesized derivatives exhibited potent and selective activity against various Mtb strains on par with the first-line drugs INH and RIF and were nontoxic to mammalian cells. Only compound **11c** showed weak antibacterial activity against *S. aureus*, while the rest of all molecules were found to be inactive on the ESKAP pathogen panel. Compounds **6a**, **6b**, **6c**, **6l**, **6m**, and **7b** exhibited excellent antimycobacterial activity with MIC of 0.06 μg/ml and can be considered the lead structures among the synthesized derivatives. Also, the compounds **6m** and **7h** exhibited excellent SI of >666 and >320, respectively. In silico studies have demonstrated that the synthesized derivatives also displayed lower binding free energy than cocrystal ligand. Also, compounds **6c**, **6g**, **6i**, **6m**, **7g**, and **7i** exhibited better interaction profiles and almost similar binding energy to the cocrystal ligand; also the ADME evaluation by the QikProp module depicted that all the molecules followed all the druggability parameters. The most potent molecules in this class may further lead to the novel antitubercular drug candidate.

4 | EXPERIMENTAL

4.1 | Chemistry

4.1.1 | General

The commercially available chemicals, such as reactants, reagents, solvents, and starting materials, were acquired from commercial providers and were used as such without further purification. The monitoring of reactions was performed by thin-layer chromatography (TLC)—MERCK precoated silica gel 60-F254 (0.5 mm) aluminum plates under UV light. Proton (^{1}H) and carbon (^{13}C) NMR spectra were acquired on Bruker's Avance 500 MHz spectrometer by using tetramethylsilane (TMS) as the internal standard and chemical shifts are reported in ppm. Chemical shifts are mentioned with reference to TMS (d 0.00 for ^{1}H NMR and ^{13}C NMR), deuterated dimethyl sulfoxide (DMSO-d_6) (d 2.50 for ^{1}H NMR, and 39.7 for ^{13}C NMR) or $CDCl_3$ (d 7.267 for ^{1}H NMR and 77.00 or 77.16 for ^{13}C NMR). Spinning multiplicities are denoted as s for singlet, brs for broad singlet, d for doublet, dd for double doublet, t for triplet, and m for multiplet. Coupling constant value (*J*) is indicated in hertz (Hz). HRMS data were carried out on Agilent QTOF mass spectrometer 6540 series instrument. Purification of final compounds by column chromatography was performed using silica gel 60–120 mesh. Melting points (MP) were noted using the Stuart® SMP30 apparatus. The InChI codes of the investigated compounds, together with observed biological activity data, are provided as Supporting Information Data.

4.1.2 | General procedure for the synthesis of 3-dimethylamino-1-(nitrophenyl)prop-2-en-1-one (2)

To the stirred solution of nitroacetophenone (24.7 mmol) in dry toluene (20 ml) in a round bottom flask, dimethylformamide-dimethyl acetal (34.6 mmol) was added. The reaction mixture was continued to stir at 110°C until TLC showed the completion of the reaction (48 h). The reaction mixture was allowed to cool to room temperature. After cooling, the solvent was evaporated under reduced pressure, and to the residue, cold brine solution 30 ml was added; the obtained precipitate was filtered and purified by recrystallization from ethanol to give the yellow solid; MP: 160–170°C. FTIR (cm^{-1}): 2919 (C–H) and 1639 (C═O). ^{1}H NMR (500 MHz, $CDCl_3$) δ 8.24 (d, J = 8.8 Hz, 2H), 8.01 (d, J = 8.8 Hz, 2H), 7.86 (d, J = 12.2 Hz, 1H), 5.68 (d, J = 12.2 Hz, 1H), 3.20 (s, 3H), and 2.97 (s, 3H); ^{13}C NMR (126 MHz, DMSO-d_6) δ 184.07, 155.70, 149.03, 146.32, 128.86, 123.84, 91.66, and 45.17; HRMS–QTOF MS/MS: m/z $[M+H]^+$ calcd for $C_{11}H_{13}N_2O_3$: 221.092; found 221.092.

4.1.3 | General procedure for the synthesis of 3-(nitrophenyl)-1*H*-pyrazole (3)

3-Dimethylamino-1-(nitrophenyl)prop-2-en-1-one (5.9 mmol) was dissolved in ethanol and water mixture (2:1). To this stirred solution hydrazine hydrate (6.5 mmol) was added dropwise at room temperature. The reaction mixture was stirred at 80°C (oil bath) for 4 h. Then, the mixture was poured on the crushed ice and the precipitated solid was filtered off, washed with brine, and dried. The dried solid was recrystallized from ethanol to give the white solid; MP: 123–125°C; ^{1}H NMR (500 MHz, DMSO-d_6) δ 13.25 (s, 1H), 8.25 (d, J = 8.5 Hz, 2H), 8.08 (d, J = 7.9 Hz, 2H), 7.88 (s, 1H), and 6.92 (d, J = 2.2 Hz, 1H); ^{13}C NMR (126 MHz, DMSO-d_6) δ 148.65, 146.74, 140.76, 131.04, 126.30, 124.52, and 103.77; FTIR (cm^{-1}): 3284 (N–H) and 3106 (C–H); HRMS–QTOF MS/MS: m/z $[M+H]^+$ calcd for $C_9H_7N_3O_2$: 190.0617; found 190.0612.

4.1.4 | General procedure for the synthesis of ethyl 2-[3-(nitrophenyl)-1*H*-pyrazol-1-yl]acetate (4)

The synthesis of ethyl 2-[3-(nitrophenyl)-1*H*-pyrazol-1-yl]acetate was done using the reported methodology.[19] The appropriately substituted ethyl bromoacetate (1.2 mmol) was added to a mixture of pyrazole (**3**) (1 mmol) and potassium carbonate (2 mmol) in acetonitrile (10 ml). The reaction mixture was stirred at 65°C (oil bath) for 15 h. After completion of the reaction indicated by TLC, the reaction mixture was poured onto crushed ice. Precipitated solid was collected by filtration, washed with water, and dried to afford the products in good purity. The obtained product was recrystallized from ethanol to give the white solid MP: 170–172°C. ^{1}H NMR (500 MHz, $CDCl_3$) δ 8.24 (d, J = 8.8 Hz, 2H), 7.96 (d, J = 8.8 Hz, 2H), 7.57 (s, 1H), 6.72 (s, 1H), 4.99 (s, 2H), 4.27 (q, J = 7.1 Hz, 2H), and 1.35–1.23 (m, 3H). ^{13}C NMR (126 MHz, $CDCl_3$) δ 167.50, 149.80, 147.19, 139.39, 132.70, 126.19, 124.07, 104.92, 77.28, 77.03, 76.78, 62.12, and 53.49; FTIR (cm^{-1}): 3120 (N–H), 2978 (C–H), and 1733 (C═O); HRMS–QTOF MS/MS: m/z $[M+H]^+$ calcd for $C_{13}H_{13}N_3O_4$: 276.0986; found 276.0985.

4.1.5 | General procedure for the synthesis of 2-[3-(nitrophenyl)-1*H*-pyrazol-1-yl]acetic acid (5)

2-[3-(Nitrophenyl)-1*H*-pyrazol-1-yl] acetic acid was obtained by hydrolysis of ethyl 2-(3-phenyl-1*H*-pyrazol-1-yl)acetate. Pyrazole acetate (**4**) (1 mmol) was added to a solution of sodium hydroxide (2 mmol) in water under stirring; after addition, the reaction mixture was stirred at room temperature for 12 h. After completion of the reaction, the resulting mixture was acidified with 3 N hydrochloric acid. The precipitate obtained was filtered and dried in a hot air oven and recrystallized from ethanol to yield the white solid; MP: 206–208°C; FTIR (cm^{-1}): 2928, 1730, and 1403; ^{1}H NMR (500 MHz, DMSO-d_6) δ 13.16 (s, 1H), 8.27 (d, J = 8.9 Hz, 2H), 8.07 (d, J = 8.9 Hz, 2H), 7.88 (d, J = 2.4 Hz, 1H), and 6.96 (s, 1H), 5.07 (s, 2H). ^{13}C NMR (126 MHz, $CDCl_3$) δ 174.68, 153.53, 151.63, 144.85, 139.22, 139.03, 131.08, 129.36, 109.76, 109.60, and 58.25; HRMS–QTOF MS/MS: m/z $[M+H]^+$ calcd for $C_{11}H_9N_3O_4$: 248.0671; found 248.0668.

4.1.6 | General procedure for the synthesis of 2-[3-(nitrophenyl)-1*H*-pyrazol-1-yl]acetamides (6a–o)

To a stirred solution of 2-[3-(nitrophenyl)-1*H*-pyrazol-1-yl]acetic acid (**5**), (0.40 mmol) in anhydrous DMF (10 ml) was added 1-(3-dimethylaminopropyl)-3-ethylcarbodiimide hydrochloride (0.56 mmol), DMAP (0.56 mmol) and corresponding amine (0.40 mmol) at room temperature and stirred at room temperature for 12–14 h until completion of the reaction. Brine solution (30 ml) was added into the reaction mixture; the resulting solid precipitate was collected by filtration, the filtered solid was washed with cold water (50 ml) and followed by cold methanol (10 ml) and dried to afford crude product. The resulting crude compound was purified by using column chromatography (*n*-hexane/EtOAc 4:1) or by recrystallization from methanol to give a pure target compound.

*2-[3-(4-Nitrophenyl)-1*H*-pyrazol-1-yl]-N-[4-(trifluoromethyl)phenyl]-acetamide (**6a**)*

Pale yellow solid; MP: 220–222°C; ^{1}H NMR (500 MHz, DMSO-d_6) δ (ppm): 10.86 (s, 1H), 8.27 (d, J = 9.0 Hz, 2H), 8.08 (d, J = 9.0 Hz, 2H), 7.95 (d, J = 2.4 Hz, 1H), 7.83 (d, J = 8.5 Hz, 2H), 7.71 (d, J = 8.7 Hz, 2H), 6.99 (d, J = 2.4 Hz, 1H), and 5.20 (s, 2H); ^{13}C NMR (126 MHz, DMSO-d_6) δ (ppm): 166.44, 148.95, 146.89, 144.74, 142.59, 140.08, 134.83, 126.72, 126.70, 126.36, 124.62, 119.63, 104.88, and 55.36; FTIR (cm^{-1}): 3068 (C–H), 1699 (C═O), and 1319 (C–F); HRMS–QTOF MS/MS: m/z $[M+H]^+$ calcd for $C_{18}H_{13}F_3N_4O_3$: 391.1018; found 391.1014.

N-*Cyclohexyl-2-[3-(4-nitrophenyl)-1*H*-pyrazol-1-yl]acetamide (**6b**)*

Cream solid; MP: 180–182°C; ^{1}H NMR (500 MHz, DMSO-d_6) δ (ppm): 8.27 (d, J = 9.0 Hz, 2H), 8.06 (d, J = 9.0 Hz, 2H), 7.84 (d, J = 2.4 Hz, 1H), 6.94 (d, J = 2.4 Hz, 1H), 4.83 (s, 2H), 2.67 (ddd, J = 11.4, 7.6, 4.0 Hz, 1H), 1.24 (s, 1H), 0.66 (q, J = 7.0 Hz, 2H), and 0.52–0.42 (m, 2H); ^{13}C NMR (126 MHz, $CDCl_3$) δ (ppm): 167.80, 148.67, 146.82, 140.19, 134.52, 126.29, 124.60, 104.68, 54.68, 48.19, 32.70, 25.69, and 24.89; FTIR (cm^{-1}): 3217 (C–H), 2937 (C–H), and 1648 (C═O); HRMS–QTOF MS/MS: m/z [M+H]$^+$ calcd for $C_{17}H_{20}N_4O_3$: 329.1614; found 329.1616.

N-*Cycloheptyl-2-[3-(4-nitrophenyl)-1*H*-pyrazol-1-yl]acetamide (**6c**)*

Cream solid; MP: 145–147°C; ^{1}H NMR (500 MHz, DMSO-d_6) δ (ppm): 8.59–8.55 (m, 1H), 8.23 (d, J = 8.0 Hz, 1H), 8.19 (d, J = 7.8 Hz, 1H), 8.15 (d, J = 9.6 Hz, 1H), 7.83 (d, J = 2.3 Hz, 1H), 7.71 (t, J = 8.0 Hz, 1H), 6.93 (d, J = 2.3 Hz, 1H), 4.85 (s, 2H), 3.80–3.72 (m, 1H), 1.83–1.76 (m, 2H), and 1.59–1.39 (m, 10H); ^{13}C NMR (126 MHz, DMSO-d_6) δ (ppm): 165.46, 148.80, 148.56, 134.37, 131.83, 122.42, 119.55, 103.87, 54.79, 50.32, 34.68, 28.27, and 24.12. FTIR (cm^{-1}): 3279 (C–H), 2930 (C–H), and 1655 (C═O); HRMS–QTOF MS/MS: m/z [M+H]$^+$ calcd for $C_{18}H_{22}N_4O_3$: 343.1770; found, 343.1774.

N-*3-Chlorophenyl-2-[3-(4-nitrophenyl)-1*H*-pyrazol-1-yl]-acetamide (**6d**)*

Yellow solid; MP: 232–234°C; ^{1}H NMR (500 MHz, DMSO-d_6) δ (ppm): 10.64 (s, 1H), 8.27 (d, J = 8.9 Hz, 2H), 8.08 (d, J = 8.9 Hz, 2H), 7.93 (d, J = 2.4 Hz, 1H), 7.81 (s, 1H), 7.48 (d, J = 7.3 Hz, 1H), 7.38 (t, J = 8.1 Hz, 1H), 7.16 (d, J = 8.0 Hz, 1H), 6.99 (d, J = 2.4 Hz, 1H), and 5.16 (s, 2H); ^{13}C NMR (126 MHz, DMSO-d_6) δ (ppm): 166.15, 148.94, 146.89, 140.45, 140.10, 134.80, 133.65, 131.09, 126.35, 124.61, 123.89, 119.20, 118.10, 104.85, and 55.34; FTIR (cm^{-1}): 3354, 2925 (C–H), 1683 (C═O), and 775 (C–Cl); HRMS–QTOF MS/MS: m/z [M+H]$^+$ calcd for $C_{17}H_{13}ClN_4O_3$: 357.0754; found, 357.0771.

N-*3-Chloro-4-fluorophenyl-2-[3-(4-nitrophenyl)-1*H*-pyrazol-1-yl]-acetamide (**6e**)*

Light yellow solid; MP: 249–251°C; ^{1}H NMR (500 MHz, DMSO-d_6) δ (ppm): 10.65 (s, 1H), 8.27 (d, J = 9.0 Hz, 2H), 8.08 (d, J = 9.0 Hz, 2H), 7.92 (d, J = 7.2 Hz, 2H), 7.52–7.48 (m, 1H), 7.41 (t, J = 9.1 Hz, 1H), 6.99 (d, J = 2.3 Hz, 1H), and 5.15 (s, 2H); ^{13}C NMR (126 MHz, DMSO-d_6) δ (ppm): 166.05, 154.78, 152.84, 148.97, 146.91, 140.09, 134.29, 126.36, 124.60, 121.20, 120.11, 119.69, 117.51, 104.86, and 55.28; FTIR (cm^{-1}): 3352, 2954 (C-H), 1687 (C═O), 754 (C═Cl), and 1324 (C–F); HRMS–QTOF MS/MS: m/z [M+H]$^+$ calcd for $C_{17}H_{12}ClFN_4O_3$: 375.0660; found, 375.0663.

N-*4-Methoxyphenyl-2-[3-(4-nitrophenyl)-1*H*-pyrazol-1-yl]-acetamide (**6f**)*

Yellow solid; MP: 200–202°C; FTIR (cm^{-1}): 3265, 2923 (C–H), 1680 (C═O), and 1242 (C–O); ^{1}H NMR (500 MHz, DMSO-d_6) δ (ppm): 10.25 (s, 1H), 8.27 (d, J = 9.0 Hz, 2H), 8.08 (d, J = 9.0 Hz, 2H), 7.92 (d, J = 2.4 Hz, 1H), 7.52 (d, J = 9.1 Hz, 2H), 6.98 (d, J = 2.4 Hz, 1H), 6.91 (d, J = 9.1 Hz, 2H), 5.10 (s, 2H), and 3.73 (s, 3H); ^{13}C NMR (126 MHz, DMSO-d_6) δ (ppm): 165.13, 155.94, 148.84, 143.32, 134.76, 132.67, 132.15, 126.33, 124.63, 121.19, 114.47, 104.78, 55.64, and 55.30; HRMS–QTOF MS/MS: m/z [M+H]$^+$ calcd for $C_{18}H_{16}N_4O_4$: 353.1250; found, 353.1266.

N-*2-Fluorophenyl-2-[3-(4-nitrophenyl)-1*H*-pyrazol-1-yl]-acetamide (**6g**)*

Light yellow solid; MP: 216–218°C; ^{1}H NMR (500 MHz, DMSO-d_6) δ (ppm): 10.20 (s, 1H), 8.28 (d, J = 8.6 Hz, 2H), 8.09 (d, J = 8.6 Hz, 2H), 7.93 (s, 2H), 7.29 (s, 1H), 7.20–7.15 (m, 2H), 6.98 (d, J = 1.5 Hz, 1H), and 5.24 (s, 2H); ^{13}C NMR (126 MHz, DMSO-d_6) δ (ppm): 166.28, 148.94, 146.90, 140.11, 134.80, 126.36, 124.97, 124.61, 116.12, 115.97, 104.84, and 55.07; FTIR (cm^{-1}): 2923 (C–H), 1673 (C═O), and 1353 (C–F); HRMS–QTOF MS/MS: m/z [M+H]$^+$ calcd for $C_{17}H_{13}FN_4O_3$: 341.1050; found, 341.1058.

N-*4-Fluorophenyl-2-[3-(4-nitrophenyl)-1*H*-pyrazol-1-yl]-acetamide (**6h**)*

Pale yellow solid; MP: 161–163°C ^{1}H NMR (500 MHz, DMSO-d_6) δ (ppm): 10.57 (s, 1H), 8.27 (d, J = 8.8 Hz, 2H), 8.08 (d, J = 8.8 Hz, 2H), 7.93 (d, J = 2.3 Hz, 1H), 7.64 (d, J = 8.9 Hz, 2H), 7.40 (d, J = 8.8 Hz, 2H), 6.99 (d, J = 2.3 Hz, 1H), and 5.15 (s, 2H); ^{13}C NMR (126 MHz, DMSO-d_6) δ (ppm): 165.63, 159.60, 148.88, 146.87, 140.13, 135.49, 134.75, 126.34, 124.60, 121.52, 121.46, 116.01, 115.83, 104.80, and 55.30. HRMS–QTOF MS/MS: m/z [M+H]$^+$ calcd for $C_{17}H_{13}FN_4O_3$: 341.1050; found, 341.1054.

N-*Naphthalene-1-yl-2-[3-(4-nitrophenyl)-1*H*-pyrazol-1-yl]-acetamide (**6i**)*

Brown solid; MP: 179–181°C; ^{1}H NMR (500 MHz, DMSO-d_6) δ (ppm): 10.42 (s, 1H), 8.30 (d, J = 8.9 Hz, 2H), 8.19 (d, J = 8.0 Hz, 1H), 8.12 (d, J = 8.8 Hz, 2H), 8.00–7.95 (m, 2H), 7.80 (d, J = 8.2 Hz, 1H), 7.74 (d, J = 7.3 Hz, 1H), 7.58 (t, J = 7.4 Hz, 2H), 7.51 (t, J = 7.8 Hz, 1H), 7.01 (d, J = 2.2 Hz, 1H), and 5.34 (s, 2H); ^{13}C NMR (126 MHz, DMSO-d_6) δ (ppm): 166.63, 148.90, 148.83, 134.71, 134.71, 131.90, 130.86, 128.68, 126.63, 126.07, 123.07, 122.53, 119.61, 104.12, and 55.23; FTIR (cm^{-1}): 3249, 3027, 2924 (C–H), and 1664 (C═O); HRMS–QTOF MS/MS: m/z [M+H]$^+$ calcd for $C_{21}H_{16}N_4O_3$: 373.1301; found, 373.1303.

N-*4-Bromophenyl-2-[3-(4-nitrophenyl)-1*H*-pyrazol-1-yl]-acetamide (**6j**)*

Dark brown solid; MP: 201–203°C; ^{1}H NMR (500 MHz, DMSO-d_6) δ (ppm): 10.47 (s, 1H), 8.21–8.18 (m, 2H), 8.00 (d, J = 9.0 Hz, 2H), 7.85 (d, J = 2.4 Hz, 1H), 7.51 (d, J = 8.9 Hz, 2H), 7.45 (d, J = 8.9 Hz, 2H), 6.91 (d, J = 2.4 Hz, 1H), and 5.07 (s, 2H); ^{13}C NMR (126 MHz, DMSO-D_6) δ (ppm): 165.89, 148.91, 146.88, 140.10, 138.40, 134.78, 132.19, 126.35, 124.61, 121.62, 115.77, 104.84, and 55.36; FTIR (cm^{-1}): 3357, 2923 (C–H), 1689 (C═O), and 745 (C–Br); HRMS–QTOF MS/MS: m/z [M+H]$^+$ calcd for $C_{17}H_{13}BrN_4O_3$: 401.0249; found, 401.0249.

*2-[3-(4-Nitrophenyl)-1H-pyrazol-1-yl]-N-phenylacetamide (**6k**)*

Whitish yellow solid; MP: 188–190°C; ^{1}H NMR (500 MHz, DMSO-d_6) δ (ppm): 10.65 (s, 1H), 8.27 (d, J = 9.0 Hz, 2H), 8.08 (d, J = 9.0 Hz, 2H), 7.92 (d, J = 7.2 Hz, 2H), 7.52–7.48 (m, 1H), 7.41 (t, J = 9.1 Hz, 1H), 6.99 (d, J = 2.3 Hz, 1H), and 5.15 (s, 2H); ^{13}C NMR (126 MHz, DMSO-d_6) δ (ppm): 165.74, 148.80, 135.43, 134.65,131.86, 130.83, 129.35, 124.12, 122.49, 119.69, 119.60, 104.05, and 55.30; FTIR (cm^{-1}): 3278, 2924 (C–H), and 1866 (C═O); HRMS–QTOF MS/MS: m/z [M+H]$^+$ calcd for $C_{17}H_{14}N_4O_3$: 323.1144; found, 323.1145.

*N-4-Morpholinophenyl-2-[3-(4-nitrophenyl)-1H-pyrazol-1-yl]-acetamide (**6l**)*

Light yellow solid; MP: 241–243°C; ^{1}H NMR (500 MHz, DMSO-d_6) δ (ppm): 10.25 (s, 1H), 8.27 (d, J = 8.93358, 2958, 1682, 1327; Hz, 2H), 8.08 (d, J = 8.9 Hz, 2H), 7.92 (d, J = 2.3 Hz, 1H), 7.48 (d, J = 9.0 Hz, 2H), 6.98 (d, J = 2.3 Hz, 1H), 6.92 (d, J = 9.1 Hz, 2H), 5.10 (s, 2H), 3.74–3.71 (m, 4H), and 3.07–3.03 (m, 4H); ^{13}C NMR (126 MHz, DMSO-d_6) δ (ppm): 164.96, 148.82, 147.95, 146.85, 140.17, 134.72, 131.25, 126.32, 124.60, 120.77, 115.91, 104.74, 66.57, 55.34, and 49.27; FTIR (cm^{-1}): 2958 (C–H), 1682 (C═O), and 1327 (C–O); HRMS–QTOF MS/MS: m/z [M+H]$^+$ calcd for $C_{21}H_{21}N_5O_4$: 408.1672; found, 408.1692.

*N-4-Chlorophenyl-2-[3-(4-nitrophenyl)-1H-pyrazol-1-yl]-acetamide (**6m**)*

Cream solid; MP: 140–142°C; ^{1}H NMR (500 MHz, DMSO-d_6) δ (ppm): 10.57 (s, 1H), 8.27 (d, J = 8.8 Hz, 2H), 8.08 (d, J = 8.8 Hz, 2H), 7.93 (d, J = 2.3 Hz, 1H), 7.64 (d, J = 8.9 Hz, 2H), 7.40 (d, J = 8.8 Hz, 2H), 6.99 (d, J = 2.3 Hz, 1H), and 5.15 (s, 2H); ^{13}C NMR (126 MHz, DMSO-d_6) δ (ppm): 165.87, 148.91, 146.88, 140.11, 137.99, 134.78, 129.28, 126.35, 124.61, 121.25, 104.83, and 79.65; FTIR (cm^{-1}): 3058, 2923 (C–H), 1690 (C═O), and 745 (C–Cl); HRMS–QTOF MS/MS: m/z [M+H]$^+$ calcd for $C_{17}H_{13}ClN_4O_3$: 357.0754; found, 357.0771.

*N-Mesityl-2-[3-(4-nitrophenyl)-1H-pyrazol-1-yl]acetamide (**6n**)*

Light brown solid; MP: 215–217°C; ^{1}H NMR (500 MHz, DMSO-d_6) δ (ppm): 10.36 (s, 1H), 8.28 (d, J = 8.8 Hz, 2H), 8.08 (d, J = 8.8 Hz, 2H), 7.92 (d, J = 2.3 Hz, 1H), 6.99 (s, 3H), 5.11 (s, 2H), 3.74 (s, 6H), and 3.63 (s, 3H); ^{13}C NMR (126 MHz, DMSO-d_6) δ (ppm): 165.54, 153.27, 148.91, 146.88, 140.13, 135.15, 134.79, 134.13, 126.33, 124.62, 104.77, 97.39, 60.58, 56.16, and 55.37; FTIR (cm^{-1}): 3058 (C–H) and 1660 (C═O); HRMS–QTOF MS/MS: m/z [M+H]$^+$ calcd for $C_{20}H_{20}N_4O_3$: 365.1614; found, 365.1590.

*N-Cyclopropyl-2-[3-(3-nitrophenyl)-1H-pyrazol-1-yl]acetamide (**7a**)*

Cream solid; MP: 205–507°C; ^{1}H NMR (500 MHz, DMSO-d_6) δ (ppm): 8.34 (d, J = 3.5 Hz, 1H), 8.27 (d, J = 8.6 Hz, 2H), 8.06 (d, J = 8.6 Hz, 2H), 7.84 (d, J = 2.1 Hz, 1H), 6.94 (d, J = 2.2 Hz, 1H), 4.83 (s, 2H), 2.67 (td, J = 7.2, 3.7 Hz, 1H), 0.66 (q, J = 6.8 Hz, 2H), and 0.45 (q, J = 4.6 Hz, 2H); ^{13}C NMR (126 MHz, DMSO-d_6) δ (ppm): 167.78, 148.68, 146.84, 140.19, 134.51, 126.30, 124.59, 104.68, 54.70, 22.84, and 6.08; FTIR (cm^{-1}): 3254, 2924 (C–H), and 1664 (C═O); HRMS–QTOF MS/MS: m/z [M+H]$^+$ calcd for $C_{14}H_{14}N_4O_3$: 287.1144; found, 287.1146.

*N-Cyclohexyl-2-[3-(3-nitrophenyl)-1H-pyrazol-1-yl]acetamide (**7b**)*

Cream-colored solid; MP: 190–192°C; ^{1}H NMR (500 MHz, DMSO-d_6) δ (ppm): 8.27 (d, J = 8.9 Hz, 2H), 8.13 (d, J = 7.7 Hz, 1H), 8.06 (d, J = 9.0 Hz, 2H), 7.84 (d, J = 2.3 Hz, 1H), 6.94 (d, J = 2.4 Hz, 1H), 4.87 (s, 2H), 3.60–3.52 (m, 1H), 1.77 (d, J = 12.2 Hz, 2H), 1.69 (d, J = 13.0 Hz, 2H), and 1.31–1.13 (m, 6H); ^{13}C NMR (126 MHz, DMSO-d_6) δ (ppm): 165.65, 148.62, 146.83, 140.22, 134.48, 126.28, 124.60, 104.64, 54.83, 48.22, 32.77, 25.62, and 24.86; FTIR (cm^{-1}): 3271, 3087 (C–H), and 1638 (C═O); HRMS–QTOF MS/MS: m/z [M+H]$^+$ calcd for $C_{17}H_{20}N_4O_3$: 329.1614; found, 329.1624.

*N-Cycloheptyl-2-[3-(3-nitrophenyl)-1H-pyrazol-1-yl]acetamide (**7c**)*

Cream solid; MP: 171–173°C; ^{1}H NMR (500 MHz, DMSO-d_6) δ (ppm): 8.27 (d, J = 8.5 Hz, 2H), 8.17 (d, J = 7.7 Hz, 1H), 8.06 (d, J = 8.5 Hz, 2H), 7.84 (d, J = 2.3 Hz, 1H), 6.94 (d, J = 2.3 Hz, 1H), 4.85 (s, 2H), 3.83–3.71 (m, 1H), 1.83–1.76 (m, 2H), and 1.60–1.38 (m, 10H); ^{13}C NMR (126 MHz, DMSO-d_6) δ (ppm): 165.38, 148.63, 146.84, 140.22, 134.48, 126.28, 124.60, 104.64, 54.86, 50.33, 34.68, 28.25, and 24.11; FTIR (cm^{-1}): 3290 and 2925 (C–H); HRMS–QTOF MS/MS: m/z [M+H]$^+$ calcd for $C_{18}H_{22}N_4O_3$: 343.1770; found, 343.1776.

*N-3-Chlorophenyl-2-[3-(3-nitrophenyl)-1H-pyrazol-1-yl]-acetamide (**7d**)*

Yellow solid; MP: 217–219°C; ^{1}H NMR (500 MHz, DMSO-d_6) δ (ppm): 10.76 (s, 1H), 8.59 (s, 1H), 8.26 (d, J = 7.7 Hz, 1H), 8.16 (d, J = 9.7 Hz, 1H), 7.93 (d, J = 2.2 Hz, 1H), 7.83 (d, J = 8.5 Hz, 2H), 7.74–7.69 (m, 3H), 6.99 (d, J = 2.2 Hz, 1H), and 5.19 (s, 2H); ^{13}C NMR (126 MHz, DMSO-d_6) δ (ppm): 166.49, 148.90, 148.81, 142.60, 135.39, 134.70, 131.88, 130.8, 126.70, 122.51, 119.64, 104.13, and 55.31; FTIR (cm^{-1}): 3027, 2924 (C–H), 755 (C–Cl), and 1681 (C═O); HRMS–QTOF MS/MS: m/z [M+H]$^+$ calcd for $C_{17}H_{13}ClN_4O_3$: 357.0754; found, 357.0758.

*N-3-Chloro-4-fluorophenyl-2-[3-(3-nitrophenyl)-1H-pyrazol-1-yl]-acetamide (**7e**)*

White brown solid; MP: 248–250°C; ^{1}H NMR (500 MHz, DMSO-d_6) δ (ppm): 10.67 (s, 1H), 8.27 (d, J = 8.9 Hz, 2H), 8.08 (d, J = 8.9 Hz, 2H), 7.92 (dd, J = 7.7, 3.4 Hz, 2H), 7.52–7.48 (m, 1H), 7.41 (t, J = 9.1 Hz, 1H), 6.99 (d, J = 2.4 Hz, 1H), and 5.15 (s, 2H); ^{13}C NMR (126 MHz, DMSO-d_6) δ (ppm): 166.05, 148.96, 146.91, 140.09, 136.25, 134.79, 126.36, 124.61, 121.19, 120.05, 117.69, 117.52, 104.86, and 55.27; FTIR (cm^{-1}): 3352, 2924 (C–H), 1687 (C═O), 1324 (C–F), and 754 (C–Cl); HRMS–QTOF MS/MS: m/z [M+H]$^+$ calcd for $C_{17}H_{12}ClFN_4O_3$: 375.0660; found, 375.0656.

*N-4-Methoxyphenyl-2-[3-(3-nitrophenyl)-1H-pyrazol-1-yl]-acetamide (**7f**)*

White brown solid; MP: 185–187°C; ^{1}H NMR (500 MHz, DMSO-d_6) δ (ppm): 10.26 (s, 1H), 8.59 (s, 1H), 8.25 (d, J = 7.8 Hz, 1H), 8.16 (d, J = 8.2 Hz, 1H), 7.91 (d, J = 2.2 Hz, 1H), 7.72 (t, J = 8.0 Hz, 1H), 7.52 (d, J = 8.9 Hz, 2H), 6.97 (d, J = 2.2 Hz, 1H), 6.91 (d, J = 9.0 Hz, 2H), 5.09 (s, 2H), and 3.73 (s, 3H); ^{13}C NMR (126 MHz, DMSO-d_6) δ (ppm): 165.19, 155.96, 148.79, 135.45, 134.61, 132.17, 131.86, 130.82, 122.47, 121.24, 119.60, 114.47, 104.02, 55.65, and 55.25; FTIR (cm^{-1}):

3254, 2920 (C–H), 1682 (C═O), and 1244 (C–O); HRMS–QTOF MS/MS: *m/z* $[M+H]^+$ calcd for $C_{18}H_{16}N_4O_4$: 353.1250; found, 353.1254.

N-*2-Fluorophenyl-2-[3-(3-nitrophenyl)-1H-pyrazol-1-yl]-acetamide (**7g**)*

Light brown solid; MP: 206–208°C; ^{1}H NMR (500 MHz, DMSO-d_6) δ (ppm): 10.20 (s, 1H), 8.28 (d, J = 8.9 Hz, 2H), 8.09 (d, J = 8.9 Hz, 2H), 7.94 (d, J = 2.3 Hz, 2H), 7.32–7.27 (m, 1H), 7.20–7.16 (m, 2H), 6.99 (d, J = 2.4 Hz, 1H), and 5.24 (s, 2H); ^{13}C NMR (126 MHz, DMSO-d_6) δ (ppm): 166.27, 154.92, 148.95, 146.90, 140.10, 134.81, 126.36, 126.05, 124.96, 124.61, 124.24, 116.05, 104.85, and 55.06; FTIR (cm^{-1}): 3320, 2924 (C–H), 1672 (C═O), and 1333 (C–F); HRMS–QTOF MS/MS: *m/z* $[M+H]^+$ calcd for $C_{17}H_{13}FN_4O_3$: 341.1050; found, 341.1054.

N-*4-Fluorophenyl-2-[3-(3-nitrophenyl)-1H-pyrazol-1-yl]-acetamide (**7h**)*

Brown solid; MP: 271–273°C; ^{1}H NMR (500 MHz, $CDCl_3$) δ (ppm): 10.47 (s, 1H), 8.39 (s, 1H), 7.75 (dd, J = 11.4, 8.1 Hz, 2H), 7.57 (d, J = 8.5 Hz, 1H), 7.34 (t, J = 7.5 Hz, 1H), 5.15 (d, J = 2.5 Hz, 2H), and 2.29 (t, J = 2.5 Hz, 1H); ^{13}C NMR (126 MHz, DMSO-d_6) δ (ppm): 165.70, 148.83, 146.85, 140.15, 135.66, 134.76, 126.34, 124.59, 121.49, 115.94, 115.84, 104.77, 55.29, and 25.34; FTIR (cm^{-1}): 3392, 3076 (C–H), 1663 (C═O), and 1327 (C–F); HRMS–QTOF MS/MS: *m/z* $[M+H]^+$ calcd for $C_{17}H_{13}FN_4O_3$: 341.1050; found, 341.1056.

N-*Naphthalen-1-yl-2-[3-(3-nitrophenyl)-1H-pyrazol-1-yl]-acetamide (**7i**)*

Cream solid; MP: 254–256°C; ^{1}H NMR (500 MHz, DMSO-d_6) δ (ppm): 10.37 (s, 1H), 8.69 (s, 1H), 8.34 (d, J = 7.8 Hz, 1H), 8.23 (t, J = 8.0 Hz, 2H), 8.02 (d, J = 8.7 Hz, 2H), 7.85 (d, J = 8.2 Hz, 1H), 7.78 (t, J = 8.0 Hz, 2H), 7.63 (dd, J = 12.2, 6.8 Hz, 2H), 7.56 (t, J = 7.8 Hz, 1H), 7.05 (d, J = 2.1 Hz, 1H), and 5.37 (s, 2H); ^{13}C NMR (126 MHz, DMSO-d_6) δ (ppm): 166.63, 148.91, 148.83, 134.71, 131.90, 130.85, 128.68, 126.53, 126.06, 123.06, 122.52, 119.62, 104.11, and 55.22; FTIR (cm^{-1}): 3209, 3083 (C–H), and 1681 (C═O); HRMS–QTOF MS/MS: *m/z* $[M+H]^+$ calcd for $C_{21}H_{16}N_4O_3$: 373.1301; found, 373.1307.

N-*4-Bromophenyl-2-[3-(3-nitrophenyl)-1H-pyrazol-1-yl]-acetamide (**7j**)*

Gray solid; MP: 230–230°C; ^{1}H NMR (500 MHz, DMSO-d_6) δ (ppm): 10.54 (s, 1H), 8.27 (d, J = 9.0 Hz, 2H), 8.07 (d, J = 9.0 Hz, 2H), 7.93 (d, J = 2.4 Hz, 1H), 7.58 (d, J = 8.9 Hz, 2H), 7.52 (d, J = 8.9 Hz, 2H), 6.98 (d, J = 2.4 Hz, 1H), and 5.14 (s, 2H); ^{13}C NMR (126 MHz, DMSO-d_6) δ (ppm): 165.89, 148.91, 146.89, 140.10, 138.40, 134.78, 132.19, 126.35, 124.61, 121.63, 115.76, 104.84, and 55.36; FTIR (cm^{-1}): 3357, 3065 (C–H), 1688 (C═O), and 746 (C–Br); HRMS–QTOF MS/MS: *m/z* $[M+H]^+$ calcd for $C_{17}H_{13}BrN_4O_3$: 403.0229; found, 403.0229.

N-*4-Fluoro-3-nitrophenyl-2-[3-(3-nitrophenyl)-1H-pyrazol-1-yl]-acetamide (**7k**)*

Dark brown solid; MP: 251–253°C; ^{1}H NMR (500 MHz, DMSO-d_6) δ (ppm): 11.05 (s, 1H), 8.27 (d, J = 8.9 Hz, 2H), 8.08 (d, J = 8.9 Hz, 2H), 7.94 (d, J = 2.2 Hz, 1H), 7.68 (dd, J = 9.0, 5.0 Hz, 2H), 7.17 (t, J = 8.9 Hz, 2H), 6.98 (d, J = 2.3 Hz, 1H), and 5.17 (s, 2H); ^{13}C NMR (126 MHz, DMSO-d_6) δ (ppm): 166.04, 148.95, 146.89, 140.08, 134.80, 126.35, 124.61, 118.13, 116.06, 108.86, 108.68, 104.86, and 55.27; FTIR (cm^{-1}): 3324, 2920 (C–H), 1693 (C═O), and 1512 (N–O); HRMS–QTOF MS/MS: *m/z* $[M+H]^+$ calcd for $C_{17}H_{12}FN_5O_5$: 386.0901; found, 386.0901.

N-*[Benzo(d)thiazol-2-yl]-2-[3-(3-nitrophenyl)-1H-pyrazol-1-yl]-acetamide (**7l**)*

Gray solid; MP: 228–230°C; ^{1}H NMR (500 MHz, DMSO-D_6) δ (ppm): 8.61–8.58 (m, 1H), 8.27 (d, J = 7.8 Hz, 1H), 8.16 (d, J = 8.2 Hz, 1H), 7.97 (dd, J = 10.4, 5.0 Hz, 2H), 7.78 (d, J = 8.0 Hz, 1H), 7.72 (s, 1H), 7.45 (t, J = 7.7 Hz, 1H), 7.32 (t, J = 8.1 Hz, 1H), 7.01 (d, J = 2.4 Hz, 1H), and 5.34 (s, 2H); ^{13}C NMR (126 MHz, DMSO-D_6) δ (ppm): 167.53, 158.46, 149.04, 148.80, 134.80, 131.92, 130.85, 126.63, 124.10, 122.57, 122.24, 121.07, 119.66, 104.29, and 54.71; FTIR (cm^{-1}): 2922, 2852 (C–H), and 1688 (C═O); HRMS–QTOF MS/MS: *m/z* $[M+H]^+$ calcd for $C_{18}H_{13}N_5O_3S$: 380.0817; found, 380.0814.

4.1.7 | General procedure for acetohydrazide synthesis (8)

To the stirred solution of **4** (1 eqv) in ethanol, hydrazine hydrate (1.5 eqv) was added dropwise. After the addition is over, the reaction mixture was stirred at 50°C for 6 h. The reaction was monitored by TLC; after completion of the reaction the ethanol was evaporated on the rota-evaporator. The semisolid residue obtained was poured on crushed ice. Solid obtained was filtered and used without purification for further reactions.

4.1.8 | General procedure for the synthesis of benzylidine acetohydrazide

To the stirred solution of **8** (1 eqv) and substituted aldehyde (1 eqv) in ethanol at room temperature, a catalytic amount of acetic acid (1 mol%) was added and the reaction mixture was stirred at 50°C till completion of the reaction (5–6 h). After completion of the reaction indicated by TLC, ethanol was evaporated under reduced pressure, and to the residue 15 ml *n*-hexane was added and filtered. The solid obtained was purified by crystallization to obtain **9a** as white solid; thus remaining molecules of hydrazide series were synthesized following a similar procedure.

N′-*4-Chlorobenzylidene-2-[3-(3,4-dimethoxyphenyl)-1H-pyrazol-1-yl]acetohydrazide (**9a**)*

White solid; MP: 147–149°C, FTIR, (cm^{-1}): 2987 (C–H), 1677 (C═O), and 762 (C–Cl). ^{1}H NMR (500 MHz, DMSO-d_6) δ 11.75 (s, 1H), 8.04 (s, 1H), 7.80–7.76 (m, 3H), 7.52 (d, J = 8.5 Hz, 2H), 7.33 (s, 2H), 6.98 (d, J = 8.4 Hz, 1H), 6.69 (s, 1H), 5.43 (s, 2H), 3.81 (s, 3H), and 3.78 (s, 3H). ^{13}C NMR (126 MHz, DMSO-d_6) δ 169.23, 150.74–150.58 (m), 149.32, 148.85, 143.17, 134.91, 133.86, 133.42, 129.34 (d, J = 11.7 Hz), 129.11, 126.91, 118.06, 112.37, 109.15, 102.81, 55.97

(d, J = 5.0 Hz), and 52.92. HRMS–QTOF MS/MS: m/z $[M+H]^+$ calcd for $C_{20}H_{20}ClN_4O_3$: 399.1224; found, 399.1220.

N′-2-Chlorobenzylidene-2-[3-(3,4-dimethoxyphenyl)-1H-pyrazol-1-yl]acetohydrazide (9b)

White solid; MP: 162–164°C; FTIR (cm^{-1}): 3197, 2941 (C–H), 1674 (C═O), and 756 (C–Cl); ^{1}H NMR (500 MHz, DMSO-d_6) δ 11.88 (s, 1H), 8.44 (s, 1H), 8.08 (dd, J = 7.5, 1.9 Hz, 1H), 7.77 (d, J = 2.2 Hz, 1H), 7.54 (dd, J = 7.9, 1.2 Hz, 1H), 7.45 (dt, J = 9.6, 6.5 Hz, 2H), 7.37 (d, J = 1.8 Hz, 1H), 7.32 (dd, J = 8.3, 1.8 Hz, 1H), 6.98 (d, J = 8.4 Hz, 1H), 6.70 (dd, J = 5.6, 2.2 Hz, 1H), 5.46 (s, 2H), 3.81 (s, 3H), and 3.78 (s, 3H); ^{13}C NMR (126 MHz, DMSO-d_6) δ 169.30, 150.73, 149.39, 148.92, 140.53, 133.83, 133.49, 131.80, 130.38, 128.07, 127.53, 126.96, 118.12, 112.47, 109.29, 102.85, 56.05, and 52.97; HRMS–QTOF MS/MS: m/z $[M+H]^+$ calcd for $C_{20}H_{19}ClN_4O_3$: 399.1224; found, 399.1220.

N′-4-Cyanobenzylidene-2-[3-(3,4-dimethoxyphenyl)-1H-pyrazol-1-yl]acetohydrazide (9c)

White solid; MP: 155–157°C; FTIR (cm^{-1}): 2924, 2864 (C–H), 1682 (C═O), and 2223 (C≡N); ^{1}H NMR (500 MHz, DMSO-d_6) δ 11.93 (s, 1H), 8.09 (s, 1H), 7.96 (d, J = 8.4 Hz, 2H), 7.92 (d, J = 7.2 Hz, 2H), 7.77 (d, J = 2.3 Hz, 1H), 7.36 (d, J = 1.9 Hz, 1H), 7.32 (dd, J = 8.3, 1.9 Hz, 1H), 6.98 (d, J = 8.4 Hz, 1H), 6.69 (t, J = 2.7 Hz, 1H), 5.46 (s, 2H), 3.81 (s, 3H), and 3.78 (s, 3H); ^{13}C NMR (126 MHz, DMSO-D_6) δ 169.54, 150.72, 149.33, 148.86, 142.54, 138.92, 133.86, 133.19, 128.21, 128.06, 126.90, 118.08, 112.39, 112.32, 109.16, 102.85, 55.99, 55.95, and 52.96; HRMS–QTOF MS/MS: m/z $[M+H]^+$ calcd for $C_{21}H_{19}N_5O_3$: 390.1566; found, 390.1565.

N′-3-Nitrobenzylidene-2-[3-(3,4-dimethoxyphenyl)-1H-pyrazol-1-yl]acetohydrazide (9d)

White solid; MP: 196–198°C; FTIR (cm^{-1}): 2924, 2854 (C–H), 1681 (C═O), and 1515 (N–O); ^{1}H NMR (500 MHz, DMSO-d_6) δ 11.93 (s, 1H), 8.56 (s, 1H), 8.28–8.22 (m, 2H), 8.18 (s, 1H), 7.77 (dd, J = 9.7, 5.1 Hz, 2H), 7.36 (d, J = 1.8 Hz, 1H), 7.32 (dd, J = 8.3, 1.9 Hz, 1H), 6.98 (d, J = 8.4 Hz, 1H), 6.70 (d, J = 2.3 Hz, 1H), 5.49 (s, 2H), 3.81 (s, 3H), and 3.78 (s, 3H); ^{13}C NMR (126 MHz, DMSO-d_6) δ 169.46, 150.73, 149.34, 148.86, 148.78, 142.22, 136.34, 133.86, 133.49, 130.87, 126.92, 124.68, 121.69, 118.08, 112.39, 109.17, 102.85, 55.99, 55.95, and 52.99; HRMS–QTOF MS/MS: m/z $[M+H]^+$ calcd for $C_{20}H_{19}N_5O_5$: 410.1464; found, 410.1462.

N′-4-Nitrobenzylidene-2-[3-(3,4-dimethoxyphenyl)-1H-pyrazol-1-yl]acetohydrazide (9e)

Orange solid; MP: 171–173°C; FTIR (cm^{-1}): 3093 (C–H), 1684 (C═O), and 1509 (N–O); ^{1}H NMR (500 MHz, DMSO-d_6) δ 11.99 (s, 1H), 8.29 (d, J = 8.6 Hz, 2H), 8.15 (s, 1H), 8.04 (d, J = 8.7 Hz, 2H), 7.78 (d, J = 2.1 Hz, 1H), 7.37–7.32 (m, 2H), 6.98 (d, J = 8.3 Hz, 1H), 6.70 (d, J = 2.2 Hz, 1H), 5.49 (s, 2H), 3.81 (s, 3H), and 3.78 (s, 3H); ^{13}C NMR (126 MHz, DMSO-d_6) δ 169.60, 150.75, 149.34, 148.92, 148.30, 142.12, 140.75, 133.87, 128.61, 128.43, 126.90, 124.49, 118.08, 112.39, 109.18, 102.88, 55.98, and 52.53; HRMS–QTOF MS/MS: m/z $[M+H]^+$ calcd for $C_{20}H_{19}N_5O_5$: 410.1464; found, 410.1462.

N′-2,3,4-Trimethoxybenzylidene-2-[3-(3,4-dimethoxyphenyl)-1H-pyrazol-1-yl]acetohydrazide (9f)

White solid; MP: 126–128°C; FTIR (cm^{-1}): 2940, 2836 (C–H), and 1259 (C–O); ^{1}H NMR (500 MHz, DMSO-d_6) δ 11.56 (s, 1H), 8.23 (s, 1H), 7.76 (d, J = 2.3 Hz, 1H), 7.64 (d, J = 8.9 Hz, 1H), 7.36 (s, 1H), 7.32 (dd, J = 8.3, 1.9 Hz, 1H), 6.98 (d, J = 8.4 Hz, 1H), 6.92 (d, J = 8.9 Hz, 1H), 6.68 (d, J = 2.3 Hz, 1H), 5.40 (s, 2H), 3.84 (s, 3H), 3.81 (s, 3H), and 3.78 (d, J = 1.7 Hz, 8H); ^{13}C NMR (126 MHz, DMSO-d_6) δ 168.50, 153.01, 148.81, 142.04, 140.49, 135.57, 134.69, 131.82, 130.81, 122.40, 121.14, 120.64,120.48, 119.55, 109.21, 104.01, 62.24, 60.97, and 56.52; HRMS–QTOF MS/MS: m/z $[M+H]^+$ calcd for $C_{23}H_{26}N_4O_6$: 455.1931; found, 455.1935.

2-[3-(3,4-Dimethoxyphenyl)-1H-pyrazol-1-yl]-N′-(3,4,5-trimethoxybenzylidene)acetohydrazide (9g)

Cream solid; MP: 145–147°C; FTIR (cm^{-1}): 2908 (C–H), 1697 (C═O), and 1260 (C–O); ^{1}H NMR (500 MHz, DMSO-d_6) δ 11.72 (s, 3H), 7.96 (s, 3H), 7.78 (s, 2H), 7.78 (s, 1H), 7.37 (d, J = 1.8 Hz, 6H), 7.07 (s, 6H), 6.98 (d, J = 8.4 Hz, 4H), 6.70 (d, J = 2.3 Hz, 3H), 5.46 (s, 6H), 3.83 (s, 9H), 3.80 (d, J = 14.8 Hz, 27H), and 3.71 (s, 10H); ^{13}C NMR (126 MHz, DMSO-d_6) δ 169.15, 153.67, 150.67, 149.34, 148.85, 148.13, 144.27, 139.63, 133.90, 129.97, 126.94, 118.05, 112.39, 109.14, 104.95, 104.73, 102.75, 60.59, 56.45, 55.99, 55.95, 53.81, and 53.07; HRMS–QTOF MS/MS: m/z $[M+H]^+$ calcd for $C_{23}H_{26}N_4O_6$: 455.1931; found, 455.1942.

N′-4-Hydroxy-3-methoxybenzylidene-2-[3-(3,4-dimethoxyphenyl)-1H-pyrazol-1-yl]acetohydrazide (9h)

White solid; MP: 160–162°C; FTIR (cm^{-1}): 3048, 2909 (C–H), 1638 (C═O), and 1216 (C–O); ^{1}H NMR (500 MHz, DMSO-d_6) δ 11.52 (s, 1H), 9.51 (s, 1H), 7.93 (s, 1H), 7.77 (s, 1H), 7.35 (d, J = 9.2 Hz, 2H), 7.31 (s, 1H), 7.11 (d, J = 8.2 Hz, 1H), 6.98 (d, J = 8.4 Hz, 1H), 6.84 (d, J = 8.1 Hz, 1H), 6.69 (d, J = 2.3 Hz, 1H), 5.42 (s, 2H), 3.84 (s, 3H), and 3.81 (s, 6H); ^{13}C NMR (126 MHz, DMSO-d_6) δ 172.41, 169.12, 164.53, 163.81, 162.56, 151.11,150.69, 149.38, 148.90, 147.04, 143.33, 133.83, 131.12, 129.72, 126.98, 118.10, 116.42, 116.24, 112.46, 109.28, 102.80, 56.00, 53.80, 52.93, and 21.48; HRMS–QTOF MS/MS: m/z $[M+H]^+$ calcd for $C_{21}H_{22}N_4O_5$: 411.1668; found, 411.1666.

N′-[4-(Benzyloxy)benzylidene]-2-[3-(3,4-dimethoxyphenyl)-1H-pyrazol-1-yl]acetohydrazide (9i)

White solid; MP: 178–180°C; FTIR (cm^{-1}): 3213, 2934 (C–H), 1671 (C═O), and 1243 (C–O); ^{1}H NMR (500 MHz, DMSO-d_6) δ 11.57 (s, 1H), 7.99 (s, 1H), 7.77 (d, J = 2.2 Hz, 1H), 7.71–7.67 (m, 2H), 7.47 (d, J = 7.3 Hz, 2H), 7.41 (dd, J = 10.1, 4.7 Hz, 2H), 7.38–7.30 (m, 4H), 7.09 (s, 1H), 6.97 (d, J = 8.4 Hz, 1H), 6.69 (dd, J = 5.7, 2.3 Hz, 1H), 5.41 (s, 2H), 5.17 (d, J = 3.4 Hz, 2H), 3.81 (s, 3H), and 3.78 (s, 3H); ^{13}C NMR (126 MHz, DMSO-d_6) δ 169.17, 159.17, 150.68, 149.38, 148.90, 144.21, 137.46, 135.91, 133.85, 130.44, 128.90, 128.34, 128.23, 128.14, 126.98, 120.59, 118.10, 117.45, 112.48, 109.28, 102.80, 69.86, 56.03, 55.99, and 52.98; HRMS–QTOF MS/MS: m/z $[M+H]^+$ calcd for $C_{27}H_{26}N_4O_4$: 471.2032; found, 471.2027.

*2-[3-(3,4-Dimethoxyphenyl)-1H-pyrazol-1-yl]-N′-[(2-oxo-1,2-dihydroquinolin-3-yl)methylene]acetohydrazide (**9j**)*

Brown solid; MP: 264–266°C; FTIR (cm^{-1}): 2970 (C–H), 1678 (C═O), and 1508 (C–O); ^{1}H NMR (500 MHz, DMSO-d_6) δ 12.06 (s, 1H), 11.84 (s, 1H), 8.57 (s, 1H), 8.30 (s, 1H), 7.81–7.75 (m, 2H), 7.55 (t, J = 7.7 Hz, 1H), 7.37–7.32 (m, 3H), 7.23 (t, J = 7.8 Hz, 1H), 6.98 (d, J = 8.4 Hz, 1H), 6.70 (d, J = 2.2 Hz, 1H), 5.50 (s, 2H), 3.81 (s, 3H), and 3.78 (s, 3H); ^{13}C NMR (126 MHz, DMSO-d_6) δ 169.26, 161.40, 150.69, 149.34, 148.85, 139.48, 135.34, 133.90, 131.64, 129.57, 129.34, 126.93, 125.58, 122.87, 119.55, 118.06, 115.64, 112.39, 109.13, 102.83, 55.99, 55.95, and 53.04.S; HRMS–QTOF MS/MS: m/z [M+H]$^+$ calcd for $C_{23}H_{21}N_5O_4$: 432.1672; found, 432.1029.

4.1.9 | Synthesis of 2-[3-(4-nitrophenyl)-1*H*-pyrazol-1-yl]acetohydrazide (10)

Synthesized by general procedure 4.1.7.

N′*-4-Chlorobenzylidene-2-[3-(4-nitrophenyl)-1H-pyrazol-1-yl]-acetohydrazide (**10a**)*

White solid; MP: 238–240°C; ^{1}H NMR (500 MHz, $CDCl_3$) δ 11.34 (s, 1H), 7.97 (d, J = 8.9 Hz, 2H), 7.73 (d, J = 8.9 Hz, 3H), 7.40 (dd, J = 20.1, 5.4 Hz, 3H), 7.12 (d, J = 8.5 Hz, 2H), 6.52 (d, J = 2.4 Hz, 1H), and 5.22 (s, 2H); ^{13}C NMR (126 MHz, DMSO-d_6) δ 168.46, 149.11, 146.85, 143.73, 140.00, 135.70, 133.33, 132.64, 128.94, 128.30, 126.01, 123.91, 104.53, and 53.31; HRMS–QTOF MS/MS: m/z [M+H]$^+$ calcd for $C_{22}H_{25}N_4O_5Cl$: 384.0863; found, 384.0861.

N′*-3,4-Dimethoxybenzylidene-2-[3-(4-nitrophenyl)-1H-pyrazol-1-yl]acetohydrazide (**10b**)*

White solid; MP: 225–227°C; ^{1}H NMR (500 MHz, DMSO-d_6) δ 11.64 (s, 1H), 8.27 (d, J = 8.8 Hz, 2H), 8.08 (d, J = 8.7 Hz, 2H), 7.97 (s, 1H), 7.92 (d, J = 2.1 Hz, 1H), 7.38 (s, 1H), 7.21 (d, J = 8.3 Hz, 1H), 7.02 (d, J = 8.3 Hz, 1H), 6.98 (s, 1H), 5.52 (s, 2H), 3.83 (s, 3H), and 3.81 (s, 3H); ^{13}C NMR (126 MHz, DMSO-d_6) δ 168.55, 151.18, 149.57, 148.62, 146.83, 144.79, 140.25, 134.81, 127.17, 126.35, 126.27, 124.58, 121.97, 112.03, 109.06, 104.84, 104.74, 56.07, 56.00, 53.42, 40.44, 40.27, 40.10, 39.94, 39.77, 39.60, and 39.43; HRMS–QTOF MS/MS: m/z [M+H]$^+$ calcd for $C_{20}H_{19}N_5O_5$: 410.1 464; found, 410.1460.

N′*-4-Methylbenzylidene-2-[3-(4-nitrophenyl)-1H-pyrazol-1-yl]-acetohydrazide (**10c**)*

White solid; MP: 217–219°C; ^{1}H NMR (500 MHz, DMSO-d_6) δ 11.67 (s, 1H), 8.27 (d, J = 9.0 Hz, 2H), 8.08 (d, J = 9.0 Hz, 2H), 8.02 (s, 1H), 7.91 (d, J = 2.4 Hz, 1H), 7.65 (d, J = 8.1 Hz, 2H), 7.28 (d, J = 8.0 Hz, 2H), 6.98 (d, J = 2.4 Hz, 1H), 5.50 (s, 2H), and 2.36 (s, 3H); ^{13}C NMR (126 MHz, DMSO-d_6) δ 168.66, 148.60, 146.82, 144.73, 140.35, 140.28, 134.80, 131.71, 129.91, 127.44, 126.28, 124.60, 104.77, 53.35, and 21.50; HRMS–QTOF MS/MS: m/z [M+H]$^+$ calcd for $C_{19}H_{17}N_5O_3$: 364.1410; found, 364.1409.

4.1.10 | Synthesis of 2-[3-(3-nitrophenyl)-1*H*-pyrazol-1-yl]acetohydrazide (11)

Synthesized as per general procedure 4.1.7.

N′*-Benzylidene-2-[3-(3-nitrophenyl)-1H-pyrazol-1-yl] acetohydrazide (**11a**)*

White solid; MP: 230–232°C; FTIR (cm^{-1}): 3091, 2971 (C–H), and 1674 (C═O); ^{1}H NMR (500 MHz, DMSO-d_6) δ 11.74 (s, 1H), 8.59 (s, 1H), 8.26 (d, J = 8.0 Hz, 1H), 8.16 (d, J = 8.2 Hz, 1H), 8.06 (s, 1H), 7.90 (d, J = 1.4 Hz, 1H), 7.76 (d, J = 6.5 Hz, 2H), 7.73 (d, J = 7.9 Hz, 2H), 7.46 (s, 2H), 6.97 (d, J = 1.4 Hz, 1H), and 5.51 (s, 2H); ^{13}C NMR (126 MHz, DMSO-d_6) δ 168.87, 148.80, 148.54, 144.60, 134.70, 134.42, 131.82, 130.82, 130.52, 129.31, 127.66, 127.46, 122.41, 119.56, 104.03, and 53.27; HRMS–QTOF MS/MS: m/z [M+H]$^+$ calcd for $C_{18}H_{15}N_5O_3$: 350.1253; found, 350.1257.

N′*-3,4-Dimethoxybenzylidene-2-[3-(3-nitrophenyl)-1H-pyrazol-1-yl]acetohydrazide (**11b**)*

White solid; MP: 115–117°C; FTIR (cm^{-1}): 2949 (C–H) and 1683 (C═O); ^{1}H NMR (500 MHz, DMSO-d_6) δ 11.63 (s, 1H), 8.60–8.59 (m, 1H), 8.26 (d, J = 7.8 Hz, 1H), 8.16 (d, J = 8.2 Hz, 1H), 7.97 (s, 1H), 7.90 (d, J = 2.3 Hz, 1H), 7.72 (t, J = 8.0 Hz, 1H), 7.39 (s, 1H), 7.22 (dd, J = 8.2, 1.7 Hz, 1H), 7.02 (d, J = 8.3 Hz, 1H), 6.97 (d, J = 2.4 Hz, 1H), 5.51 (s, 2H), and 3.82 (d, J = 10.3 Hz, 6H); ^{13}C NMR (126 MHz, DMSO-d_6) δ 168.65, 151.15, 149.56, 148.81, 148.50, 144.64, 135.58, 134.64, 131.80, 130.82, 127.18, 122.40, 121.97, 119.54, 111.97, 108.97, 103.97, 56.02, and 53.36; HRMS–QTOF MS/MS: m/z [M+H]$^+$ calcd for $C_{20}H_{19}N_5O_5$: 410.1464; found, 410.1468.

N′*-2,3,4-Trimethoxybenzylidene-2-[3-(3-nitrophenyl)-1H-pyrazol-1-yl]acetohydrazide (**11c**)*

White solid; MP: 175–179°C; FTIR (cm^{-1}): 3095, 2941 (C–H), and 1677 (C═O); ^{1}H NMR (500 MHz, DMSO-d_6) δ 11.60 (s, 1H), 8.60–8.58 (m, 1H), 8.25 (d, J = 10.8 Hz, 2H), 8.16 (d, J = 8.2 Hz, 1H), 7.89 (d, J = 2.3 Hz, 1H), 7.71 (d, J = 8.0 Hz, 1H), 7.65 (d, J = 8.9 Hz, 1H), 6.97 (d, J = 2.3 Hz, 1H), 6.93 (d, J = 8.9 Hz, 1H), 5.47 (s, 2H), 3.86 (d, J = 2.2 Hz, 3H), 3.85 (s, 3H), and 3.79 (s, 3H); ^{13}C NMR (126 MHz, DMSO-d_6) δ 168.52, 155.60, 153.01, 148.81, 148.50, 142.04, 140.49, 135.57, 134.69, 131.82, 130.81, 122.40, 121.14, 120.58, 119.55, 109.21, 104.01, 62.24, 60.97, 56.52, and 53.28; HRMS–QTOF MS/MS: m/z [M+H]$^+$ calcd for $C_{21}H_{21}N_5O_6$: 440.1571; found, 440.1573.

4.2 | Pharmacological/biological assays

4.2.1 | Antibiotic susceptibility testing against mycobacteria

Antimycobacterial susceptibility testing was carried out on newly synthesized compounds by using broth microdilution assay.[41,42] Stock solutions (10 mg/ml) of test and control compounds were

prepared in DMSO and stored at −20°C. Mycobacterial cultures were inoculated in Middlebrook 7H9 enriched (Difco; Becton) media supplemented with 10% ADC-Tween-80 (bovine serum albumin, dextrose, 0.2% glycerol, and 0.05% Tween-80) and OD_{600} of the cultures was measured, followed by dilution to achieve ~10^6 CFU/ml.[35] The newly synthesized compounds were tested from 64 to 0.5 mg/l in a two-fold serial diluted fashion with 2.5 µl of each concentration added per well of a 96-well round-bottom microtitre plate. Later, 97.5 µl of bacterial suspension was added to each well containing the test compound along with appropriate controls. Presto blue (Thermo Fisher Scientific) resazurin-based dye was used for the visualized identification of active compounds. MIC of active compound was determined as the lowest concentration of compound that inhibited visible growth after the incubation period. For each compound, MIC determinations were replicated three times using duplicate samples. The MIC plates were incubated at 37°C for 7 days for Mtb and 48 h for other mycobacterial pathogens.

4.2.2 | Antibiotic susceptibility testing against ESKAP pathogen panel

Antibiotic susceptibility testing was carried out on the newly synthesized compounds by determining the MIC with reference to the standard CLSI guidelines.[43,44] MIC is defined as the minimum concentration of compound at which visible bacterial growth is inhibited. Bacterial cultures were grown in Mueller–Hinton cation supplemented broth. Optical density (OD_{600}) of the cultures was measured, followed by dilution for ~10^6 CFU/ml. This inoculum was added into a series of test wells in a microtiter plate that contained various concentrations of the compound under test ranging from 64 to 0.03 mg/ml. Controls, that is, cells alone and media alone (without compound + cells) and levofloxacin used as a reference standard. Plates were incubated at 37°C for 16–18 h, followed by observations of MIC values by the absence or presence of visible growth. For each compound, MIC determinations were performed independently three times using duplicate samples each time.

4.2.3 | Cell cytotoxicity assay

The newly synthesized compounds with good activity were screened for their cell toxicity against Vero cells using MTT assay.[45] Approximately 10^3 cells/well were seeded in a 96-well plate and incubated at 37°C with a 5% CO_2 atmosphere. After 24 h, the compound was added, ranging from 100 to 5 mg/l and incubated for 72 h at 37°C with a 5% CO_2 atmosphere. After the incubation was over, MTT was added at 5 mg/l in each well, incubated at 37°C for a further 4 h, the residual medium was discarded, 0.1 ml of DMSO was added to solubilize the formazan crystals and OD was taken at 540 nm for the calculation of CC_{50}. CC_{50} is defined as the lowest concentration of the compound, which leads to a 50% reduction in cell viability. Doxorubicin was used as a positive control and each experiment was repeated in triplicate.

4.3 | Molecular docking

The structures of ligands were drawn in ChemBioDraw Ultra 14.0. and prepared for docking by use of the Ligprep module of Schrödinger Suite 19.4. The required target protein crystal structure was accrued from the RSCB PDB site. Molecular docking studies were performed against Mtb enzyme various surface proteins KasA (PDB ID: 5W2Q), DprE1 (PDB ID: 4P8H), InhA (PDB ID: 4TZK), and MmpL3 (PDB ID: 6ajj). With the aid of Protein Preparation Wizard of Schrödinger Suite 19.4, the target protein was prepared. The prepared protein was optimized and minimized using the algorithm OPLS3 (optimized potential for liquid simulations) force field and followed by the Glide Grid Generation panel in which the Glide receptor grid was generated. Finally, all the prepared test ligands were docked by using Glide's extra precision (XP) mode of docking calculations. On the basis of the XP Glide scoring function and root mean square deviation, parameters were implemented for getting the best-ranked compounds and the specific ligand–protein binding interactions. Similarly, the in silico ADME properties were calculated by the use of the Qikprop module of the Schrödinger Suite 19.

ACKNOWLEDGMENTS

Nikhil B. Gaikwad conveys his cordial thanks to DoP, Ministry of Chemicals and Fertilizers, Govt. of India, for the award of NIPER fellowship. Grace Kaul thanks DST-INSPIRE for her fellowship and Manjulika Shukla thanks the University Grants Commission for her fellowship. The manuscript has a NIPER-H acknowledgment (no. NIPER-H/2020/M079).

CONFLICTS OF INTERESTS

The authors declare that there are no conflicts of interests.

ORCID

Nikhil B. Gaikwad https://orcid.org/0000-0002-1103-3786
Srinivas Nanduri http://orcid.org/0000-0002-6671-2022
Arunava Das Gupta https://orcid.org/0000-0001-9014-1904
Sidharth Chopra https://orcid.org/0000-0001-8823-6074
Madhavi V. Yaddanapudi https://orcid.org/0000-0002-9813-8694

REFERENCES

[1] A. Talwar, R. Stewart, S. P. Althomsons, *Morb. Mortal. Wkly. Rep.* **2020**, *69*, 1104.
[2] E. S. Zuniga, J. Early, T. Parish, *Future Microbiol.* **2015**, *10*, 217. https://doi.org/10.2217/FMB.14.125
[3] Global tuberculosis report-2019. World Health Organization, Geneva, Switzerland **2019**, Ch. 3.
[4] India TB Report-2019, Central TB Division, New Delhi, India **2019**. Ch 2.
[5] R. S. Keri, S. A. Patil, *Biomed. Pharmacother.* **2014**, *68*, 1161.
[6] Z. Zong, W. Jing, J. Shi, T. Zhang, F. Huo, Y. Shang, Q. Liang, H. Huang, Y. Pang, *Antimicrob. Agents Chemother.* **2018**, *62*, e00165.
[7] J. W. Jeong, S. J. Jung, H. H. Lee, Y. Z. Kim, T. K. Park, Y. L. Cho, S. E. Chae, S. Y. Baek, S. H. Woo, H. S. Lee, J. H. Kwak, *Antimicrob. Agents Chemother.* **2010**, *54*, 5359.
[8] S. Amaroju, M. N. Kalaga, S. Srinivasarao, A. Napiórkowska, E. Augustynowicz-Kopeć, S. Murugesan, S. Chander, R. Krishnan, K. V. G. C. Sekhar, *New J. Chem.* **2017**, *41*, 347.

[9] N. R. Emmadi, C. Bingi, S. S. Kotapalli, R. Ummanni, J. B. Nanubolu, K. Atmakur, *Bioorg. Med. Chem. Lett.* **2015**, *25*, 2918.
[10] P. Horrocks, M. R. Pickard, H. H. Parekh, S. Patel, R. B. Pathak, *Org. Biomol. Chem.* **2013**, *11*, 4891.
[11] P. Samadhiya, R. Sharma, S. K. Srivastava, S. D. Srivastava, *Chin. J. Chem.* **2011**, *29*, 1745.
[12] H. S. Sutherland, A. Blaser, I. Kmentova, S. G. Franzblau, B. Wan, Y. Wang, Z. Ma, B. D. Palmer, W. A. Denny, A. M. Thompson, *J. Med. Chem.* **2010**, *53*, 855.
[13] P. Aragade, M. Palkar, P. Ronad, D. Satyanarayana, *Med. Chem. Res.* **2013**, *22*, 2279.
[14] R. B. Pathak, P. T. Chovatia, H. H. Parekh, *Bioorg. Med. Chem. Lett.* **2012**, *22*, 5129.
[15] R. Šink, I. Sosic, M. Živec, R. Fernandez-Menendez, S. Turk, S. Pajk, D. Alvarez-Gomez, E. M. Lopez-Roman, C. Gonzales-Cortez, J. Rullas-Triconado, I. Angulo-Barturen, *J. Med. Chem.* **2015**, *58*, 613.
[16] N. Nayak, J. Ramprasad, U. Dalimba, *J. Heterocycl. Chem.* **2017**, *54*, 171.
[17] V. Rachakonda, M. Alla, S. S. Kotipalli, R. Ummani, *Eur. J. Med. Chem.* **2013**, *70*, 536.
[18] R. S. Upadhayaya, S. V. Lahore, A. Y. Sayyed, S. S. Dixit, P. D. Shinde, J. Chattopadhyaya, *Org. Biomol. Chem.* **2010**, *8*, 2180.
[19] F. S. Macchi, K. Pissinate, A. D. Villela, B. L. Abbadi, V. Rodrigues-Jr, D. D. Nabinger, S. Altenhofen, N. Sperotto, A. da Silva Dadda, F. T. Subtil, T. F. de Freitas, *Eur. J. Med. Chem.* **2018**, *155*, 153.
[20] R. Ramesh, R. D. Shingare, V. Kumar, A. Anand, B. Swetha, S. Veeraraghavan, S. Viswanadha, R. Ummanni, R. Gokhale, D. S. Reddy, *Eur. J. Med. Chem.* **2016**, *122*, 723.
[21] R. R. Kondreddi, J. Jiricek, S. P. Rao, S. B. Lakshminarayana, L. R. Camacho, R. Rao, M. Herve, P. Bifani, N. L. Ma, K. Kuhen, A. Goh, *J. Med. Chem.* **2013**, *56*, 8849.
[22] J. Stec, O. K. Onajole, S. Lun, H. Guo, B. Merenbloom, G. Vistoli, W. R. Bishai, A. P. Kozikowski, *J. Med. Chem.* **2016**, *59*, 6232.
[23] O. K. Onajole, M. Pieroni, S. K. Tipparaju, S. Lun, J. Stec, G. Chen, H. Gunosewoyo, H. Guo, N. C. Ammerman, W. R. Bishai, A. P. Kozikowski, *J. Med. Chem.* **2013**, *56*, 4093.
[24] S. M. Riyadh, *Molecules* **2011**, *16*, 1834.
[25] F. A. Rosa, P. Machado, P. S. Vargas, H. G. Bonacorso, N. Zanatta, M. A. Martins, *Synlett* **2008**, *2008*, 1673.
[26] N. H. Metwally, G. H. Elgemeie, P. G. Jones, *Acta Crystal. Sec. E: Crystal. Comm.* **2020**, *76*, 481.
[27] M. Andrés, M. Bravo, M. A. Buil, M. Calbet, M. Castillo, J. Castro, P. Eichhorn, M. Ferrer, M. D. Lehner, I. Moreno, R. S. Roberts, *Eur. J. Med. Chem.* **2014**, *71*, 168.
[28] K. Pissinate, A. D. Villela, V. Rodrigues-Jr, B. C. Giacobbo, E. S. Grams, B. L. Abbadi, R. V. Trindade, L. Roesler Nery, C. D. Bonan, D. F. Back, M. M. Campos, *ACS Med. Chem. Lett.* **2016**, *7*, 235.
[29] B. C. Giacobbo, K. Pissinate, V. Rodrigues-Jr, A. D. Villela, E. S. Grams, B. L. Abbadi, F. T. Subtil, N. Sperotto, R. V. Trindade, D. F. Back, M. M. Campos, *Eur. J. Med. Chem.* **2017**, *126*, 491.
[30] P. S. Shirude, P. Madhavapeddi, M. Naik, K. Murugan, V. Shinde, R. Nandishaiah, J. Bhat, A. Kumar, S. Hameed, G. Holdgate, G. Davies, *J. Med. Chem.* **2013**, *56*, 8533.
[31] L. Encinas, H. O'Keefe, M. Neu, M. J. Remuiñán, A. M. Patel, A. Guardia, C. P. Davie, N. Pérez-Macías, H. Yang, M. A. Convery, J. A. Messer, *J. Med. Chem.* **2014**, *57*, 1276.
[32] G. S. Pedgaonkar, J. P. Sridevi, V. U. Jeankumar, S. Saxena, P. B. Devi, J. Renuka, P. Yogeeswari, D. Sriram, *Eur. J. Med. Chem.* **2014**, *86*, 613.
[33] L. A. Spagnuolo, S. Eltschkner, W. Yu, F. Daryaee, S. Davoodi, S. E. Knudson, E. K. Allen, J. Merino, A. Pschibul, B. Moree, N. Thivalapill, *J. Am. Chem. Soc.* **2017**, *139*, 3417.
[34] U. C. Kumar, S. K. BVS, S. Mahmood, P. K. Sahu, S. Pulakanam, L. Ballell, D. Alvarez-Gomez, S. Malik, S. Jarp, *Fut. Med. Chem.* **2013**, *5*, 249.
[35] T. Štular, S. Lešnik, K. Rožman, J. Schink, M. Zdouc, A. Ghysels, F. Liu, C. C. Aldrich, V. J. Haupt, S. Salentin, S. Daminelli, *J. Med. Chem.* **2016**, *59*, 11069.
[36] F. Ntie-Kang, *SpringerPlus* **2013**, *2*, 353.
[37] C. A. Lipinski, *Drug Discov. Today: Technol.* **2004**, *1*, 337.
[38] G. R. Bickerton, G. V. Paolini, J. Besnard, S. Muresan, A. L. Hopkins, *Nat. Chem.* **2012**, *4*, 90.
[39] D. E. Clark, S. D. Pickett, *Drug Discov. Today* **2000**, *5*, 49.
[40] O. Ursu, A. Rayan, A. Goldblum, T. I. Oprea, *Wiley Interdiscip. Rev.: Comput. Mol. Sci.* **2011**, *1*, 760.
[41] M. Pandey, A. K. Singh, R. Thakare, S. Talwar, P. Karaulia, A. Dasgupta, S. Chopra, A. K. Pandey, *Sci. Rep.* **2017**, *7*, 1.
[42] I. Wiegand, K. Hilpert, R. E. W. Hancock, *Nat. Protoc.* **2008**, *3*, 163.
[43] *Methods for dilution antimicrobial susceptibility tests for bacteria that grow aerobically*, 9th ed, CLSI Document M7-A9, Clinical and Laboratory Standards Institute, Wayne, PA **2012**.
[44] J. H. Jorgensen, J. F. Hindler, L. B. Reller, M. P. Weinstein, *Clin. Infect. Dis.* **2007**, *44*, 280.
[45] S. Patel, N. Gheewala, A. Suthar, A. Shah, *Int. J. Pharm. Pharm. Sci.* **2009**, *1*, 38.

SUPPORTING INFORMATION

Additional Supporting Information may be found online in the supporting information tab for this article.

How to cite this article: Gaikwad NB, Nirmale K, Sahoo SK, et al. Design, synthesis, in silico, and in vitro evaluation of 3-phenylpyrazole acetamide derivatives as antimycobacterial agents. *Arch Pharm*. 2020;e2000349.
https://doi.org/10.1002/ardp.202000349